COLOR

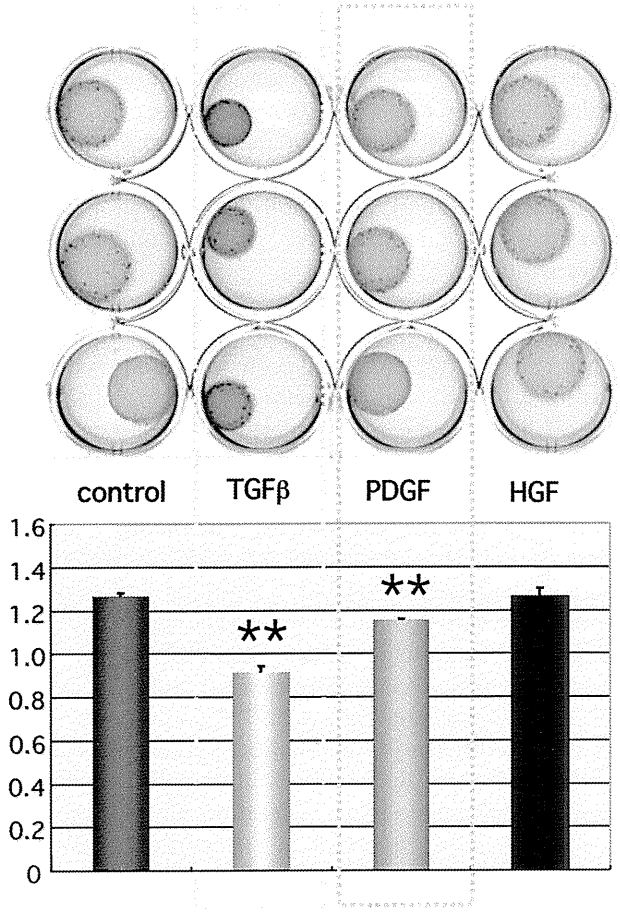

Fig. 4. Contraction of collagen gel embedded with hyalocytes. A collagen gel embedded with hyalocytes was stimulated with cytokines, such as TGF-β, platelet-derived growth factor (PDGF), or hepatocyte growth factor (HGF), and the size of the collagen gel was measured after 24 hours. The contraction of gel was significantly enhanced by TGF-β or PDGF (**$P < 0.01$). Reproduced with permission from Sakamoto.[10]

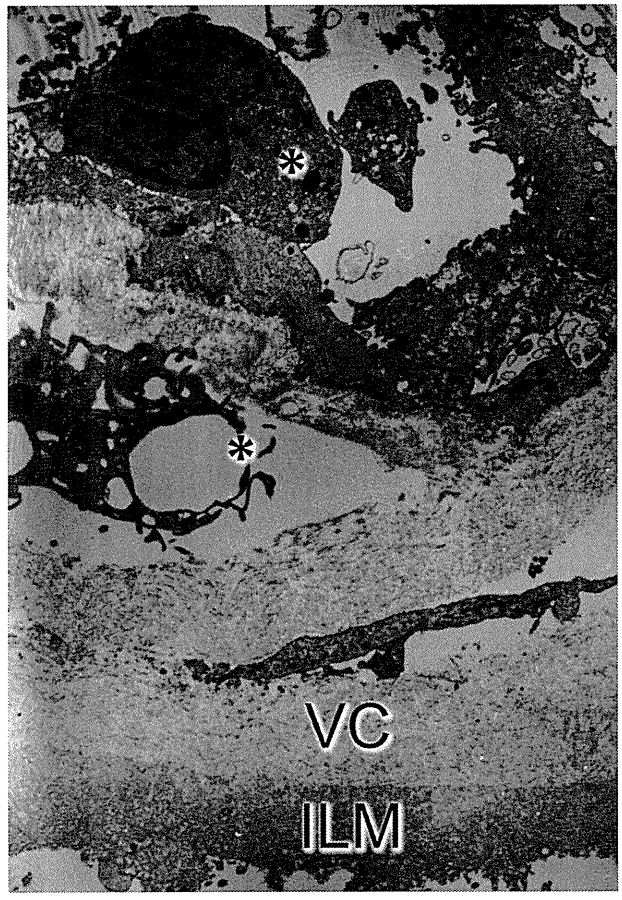

Fig. 5. Transmission electron microscopic photograph of surgically removed internal limiting membrane (ILM) from the eye of ERM. Macrophage-like cells (*) are present on the vitreous cortex (VC) and ILM. They are presumably hyalocytes. Reproduced with permission from Sakamoto[10] (original magnification, ×1800).

maneuver itself is not necessarily easy and recurrence is not rare. Adjunctive use of triamcinolone acetonide in vitrectomy is beneficial to remove these membranes securely and effectively.[53,54] Although this procedure is not always necessary in most of the cases, it might be beneficial for selected cases to reduce the incidence of postoperative preretinal fibrotic complications.[54] Complete removal of ERM together with internal limiting membrane resulted in a lower recurrence rate than incomplete removal, probably because the residual hyaloid or membrane becomes a scaffold of cell proliferation and ECM production by these cells.[55] If the residual hyaloid or internal limiting membrane is left alone without any cells, recurrence, namely reproduction of ECM by cellular elements after surgery, will not occur.

There are novel pharmacologic approaches to the disease. In an in vitro study, Rho and ROCK were found to play an important role in phosphorylation of the myosin light chain and the subsequent contraction; thus, a specific Rho kinase (ROCK) inhibitor fasudil could block contraction of collagen gel embedded with hyalocytes.[36] In rabbits, fasudil significantly inhibited the progression of experimental proliferative vitreoretinopathy without affecting the viability of retinal cells. ROCK, a key downstream mediator of TGF-β and other factors, might become a unique therapeutic target.[36] Of course, there is a distance between an animal study and the bedside; however, a pharmacologic approach to modulate hyalocytes might be a novel treatment of intraocular diseases.

Summary

As described above, there is no strict definition of "hyalocytes," but cells located at the periphery of vitreous cavity are called hyalocytes. The accumulating evidence shows that these hyalocytes can act as

COLOR

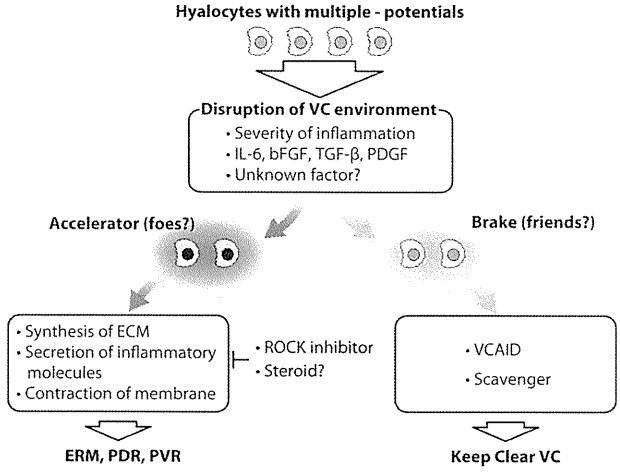

Fig. 6. Schema of possible roles of hyalocytes in ocular pathology. Hyalocytes are residual cells in vitreous cavity (VC) with multiple potentials. In the disruption of the VC environment, hyalocytes may act as an accelerator or a brake to destroy the clear vitreous dependent on unknown mechanisms. IL-6, interleukin-6; bFGF, basic fibroblast growth factor; PDGF, platelet-derived growth factor; PDR, proliferative diabetic retinopathy; PVR, proliferative vitreoretinopathy.

"friends" to keep the vitreous cavity clear by inhibiting immune reaction through vitreous cavity–associated immune deviation. At the same time, hyalocytes can act as "foes" by producing inflammatory cytokines and ECM followed by contraction of the membrane. Unfortunately, at present, it is difficult to tell what makes hyalocytes "friends" or "foes" (Figure 6). Further studies to answer this question might provide a key to a better understanding of microenvironment of the vitreous cavity and to developing an effective treatment for intraocular diseases.

F6

Key words: antigen-presenting cells, fibronectin, macular edema, VCAID, vitrectomy.

References

AQ : 4

1. Green WR, Seberg J. In: Ryan SJ, ed. Retina. 4th ed. St Louis, MO: Mosby; 2006:1921–1989.
2. Szirimai JA, Balazs EA. Studies on the structure of the vitreous body. III. Cells in the cortical layer. AMA Arch Ophthalmol 1958;59:34–48.
3. Hamburg A. Some investigations on the cells of the vitreous body. Ophthalmologica 1959;138:81–107.
4. Balazs EA, Toth LZJ, Eeckl EA, Mitchel AP. Studies on the structure of the vitreous body. XII. Cytological and histochemical studies on the cortical tissue layer. Exp Eye Res 1964; 3:57–71.
5. Sebag J. The vitreous. In: Hart WM Jr, ed. Adler's Physiology of the Eye. 9th ed. St Louis, MO: Mosby Year Book; 1992: 268–347.
6. Gloor BP. Development of the vitreous body and zonula. Graefes Arch Clin Exp Ophthalmol 1973;187:21–44.
7. Salu P, Claeskens W, De Wilde A, et al. Light and electron microscopic studies of the rat hyalocyte after perfusion fixation. Ophthalmic Res 1985;17:125–130. AQ : 5
8. Uehara M, Imagawa T, Kitagawa H. Morphological studies of the hyalocytes in the chicken eye: scanning electron microscopy and inflammatory response after the intravitreous injection of carbon particles. J Anat 1996;188:661–669.
9. Zhu M, Provis JM, Penfold PL. The human hyaloid system: cellular phenotypes and inter-relationships. Exp Eye Res 1999; 68:553–563.
10. Sakamoto T. Cell biology of hyalocytes. Nippon Ganka Gakkai Zasshi 2003;107:866–882.
11. Noda Y, Hata Y, Hisatomi T, et al. Functional properties of hyalocytes under PDGF-rich conditions. Invest Ophthalmol Vis Sci 2004;45:2107–2114.
12. Matsumoto H, Yamanaka I, Hisatomi T, et al. Triamcinolone acetonide-assisted pars plana vitrectomy improves residual posterior vitreous hyaloid removal: ultrastructural analysis of the inner limiting membrane. Retina 2007;27:174–179.
13. Ueno A, Enaida H, Hata Y, et al. Long-term clinical outcomes and therapeutic benefits of triamcinolone-assisted pars plana vitrectomy for proliferative vitreoretinopathy: a case study. Eur J Ophthalmol 2007;17:392–398.
14. Gandorfer A, Scheler R, Haritoglou C, et al. Pathology of the macular hole rim in flat-mounted internal limiting membrane specimens. Retina 2009;29:1097–1105.
15. Hogan MJ, Alvadadr JA, Weddel JE. Histology of the Human Eye. Philadelphia, PA: WB Sanders; 1971.
16. Qiao H, Hisatomi T, Sonoda KH, et al. The characterisation of hyalocytes: the origin, phenotype, and turnover. Br J Ophthalmol 2005;89:513–517.
17. Balazs EA, Toth LZ, Ozanics V. Cytological studies on the developing vitreous as related to the hyaloid vascular vessel system. Graefes Arch Clin Exp Ophthalmol 1980;213:71–85.
18. Saga T, Tagawa Y, Takeuchi T, et al. Electron microscopic study of cells in vitreous of guinea pig. Jpn J Ophthalmol 1984; 28:239–247.
19. Ogawa K. Scanning electron microscopic study of hyalocytes in the guinea pig eye. Arch Histol Cytol 2002;65:263–268.
20. Grabner G, Boltz G, Förster O. Macrophage-like properties of human hyalocytes. Invest Ophthalmol Vis Sci 1980;19: 333–340.
21. Jacobson B. Degradation of glycosaminoglycans by extracts of calf vitreous hyalocytes. Exp Eye Res 1984;39:373–385.
22. Lazarus HS, Hageman GS. In situ characterization of the human hyalocyte. Arch Ophthalmol 1994;112:1356–1362.
23. Schönfeld CL. Hyalocytes inhibit retinal pigment epithelium cell proliferation in vitro. Ger J Ophthalmol 1996;5: 224–228.
24. van Meurs JC, Sorgente N, Gauderman WJ, Ryan SJ. Clearance rate of macrophages from the vitreous in rabbits. Curr Eye Res 1990;9:683–686.
25. Gloor BP. Mitotic activity in the cortical vitreous cells (hyalocytes) after photocoagulation. Invest Ophthalmol 1969;8:633–646.
26. Haddad A, André JC. Hyalocyte-like cells are more numerous in the posterior chamber than they are in the vitreous of the rabbit eye. Exp Eye Res 1998;66:709–718.
27. Newsome DA, Linsenmayer TF, Trelstad RL. Vitreous body collagen. Evidence for a dual origin from the neural retina and hyalocytes. J Cell Biol 1976;71:59–67.
28. Osterlin SE, Jacobson B. The synthesis of hyaluronic acid in vitreous. I. Soluble and particulate transferases in hyalocytes. Exp Eye Res 1968;7:497–510.

29. Rittig M, Flügel C, Prehm P, Lütjen-Drecoll E. Hyaluronan synthase immunoreactivity in the anterior segment of the primate eye. Graefes Arch Clin Exp Ophthalmol 1993;231: 313–317.
30. Nishitsuka K, Kashiwagi Y, Tojo N, et al. Hyaluronan production regulation from porcine hyalocyte cell line by cytokines. Exp Eye Res 2007;85:539–545.
31. Sommer F, Pollinger K, Brandl F, et al. Hyalocyte proliferation and ECM accumulation modulated by bFGF and TGF-beta1. Graefes Arch Clin Exp Ophthalmol 2008;246:1275–1284.
32. Schaefer T, Roux M, Stuhlsatz HW, et al. Glycosaminoglycans modulate cell-matrix interactions of human fibroblasts and endothelial cells in vitro. J Cell Sci 1996;109:479–488.
33. Kohno RI, Hata Y, Kawahara S, et al. Possible contribution of hyalocytes to idiopathic epiretinal membrane formation and its contraction. Br J Ophthalmol 2009;93:1020–1026.
34. Kita T, Hata Y, Kano K, et al. Transforming growth factor-beta2 and connective tissue growth factor in proliferative vitreoretinal diseases: possible involvement of hyalocytes and therapeutic potential of Rho kinase inhibitor. Diabetes 2007; 56:231–238.
35. Kampik A, Green WR, Michels RG, Nase PK. Ultrastructural features of progressive idiopathic epiretinal membrane removed by vitreous surgery. Am J Ophthalmol 1980;90: 797–809.
36. Kita T, Hata Y, Arita R, et al. Role of TGF-beta in proliferative vitreoretinal diseases and ROCK as a therapeutic target. Proc Natl Acad Sci U S A 2008;105:17504–17509.
37. Sebag J. Anomalous posterior vitreous detachment: a unifying concept in vitreo-retinal disease. Graefes Arch Clin Exp Ophthalmol 2004;242:690–698.
38. Sebag J, Gupta P, Rosen RR, et al. Macular holes and macular pucker: the role of vitreoschisis as imaged by optical coherence tomography/scanning laser ophthalmoscopy. Trans Am Ophthalmol Soc 2007;105:121–129.
39. Stein-Streilein J. Immune regulation and the eye. Trends Immunol 2008;29:548–554.
40. Streilein JW. Ocular immune privilege: therapeutic opportunities from an experiment of nature. Nat Rev Immunol 2003;3: 878–889.
41. Streilein JW, Okamoto S, Hara Y, et al. Blood-borne signals that induce anterior chamber-associated immune deviation after intracameral injection of antigen. Invest Ophthalmol Vis Sci 1997;38:2245–2254.
42. Sonoda KH, Sakamoto T, Qiao H, et al. The analysis of systemic tolerance elicited by antigen inoculation into the vitreous cavity: vitreous cavity-associated immune deviation. Immunology 2005;116:390–399.
43. Tkachuk VA, Plekhanova OS, Parfyonova YV. Regulation of arterial remodeling and angiogenesis by urokinase-type plasminogen activator. Can J Physiol Pharmacol 2009;87: 231–251.
44. Hata Y, Sassa Y, Kita T, et al. Vascular endothelial growth factor expression by hyalocytes and its regulation by glucocorticoid. Br J Ophthalmol 2008;92:1540–1544.
45. Sakamoto T, Hinton DR, Sakamoto H, et al. Collagen gel contraction induced by retinal pigment epithelial cells and choroidal fibroblasts involves the protein kinase C pathway. Curr Eye Res 1994;13:451–459.
46. Hirayama K, Hata Y, Noda Y, et al. The involvement of the rho-kinase pathway and its regulation in cytokine-induced collagen gel contraction by hyalocytes. Invest Ophthalmol Vis Sci 2004; 45:3896–3903.
47. Wiedemann P, Kohlmann H. Perioperative analysis of vitreous cell components by immunoimpression cytology. Graefes Arch Clin Exp Ophthalmol 1996;123:463–466.
48. Gandorfer A, Rohleder M, Grosselfinger S, et al. Epiretinal pathology of diffuse diabetic macular edema associated with vitreomacular traction. Am J Ophthalmol 2005;139: 638–652.
49. Kampik A, Kenyon KR, Michels RG, et al. Epiretinal and vitreous membranes: comparative study of 56 cases. Arch Ophthalmol 1981;99:1445–1454.
50. Faulborn J, Dunker S, Bowald S. Diabetic vitreopathy: findings using the celloidin embedding technique. Ophthalmologica 1998;212:369–376.
51. Kishi S, Numaga T, Yamazaki, S. Structure of the inner retinal surface in simple diabetic retinopathy. Jpn J Ophthalmol 1982; 26:141–149.
52. Hisatomi T, Enaida H, Sakamoto T, et al. A new method for comprehensive bird's-eye analysis of the surgically excised internal limiting membrane. Am J Ophthalmol 2005;139: 1121–1122.
53. Enaida H, Hata Y, Ueno A, et al. Possible benefits of triamcinolone-assisted pars plana vitrectomy for retinal diseases. Retina 2003;23:764–770.
54. Sakamoto T, Ishibashi T. Visualizing vitreous in vitrectomy by triamcinolone. Graefes Arch Clin Exp Ophthalmol 2009;247: 1153–1163.
55. Shimada H, Nakashizuka H, Hattori T, et al. Double staining with brilliant blue G and double peeling for epiretinal membranes. Ophthalmology 2009;116:1370–1376.

Laboratory Investigation (2011), 1–14

NSAIDs inhibit neovascularization of choroid through HO-1-dependent pathway

Narimasa Yoshinaga[1], Noboru Arimura[1], Hiroki Otsuka[1], Ko-ichi Kawahara[2], Teruto Hashiguchi[2], Ikuro Maruyama[3] and Taiji Sakamoto[1]

Intraocular neovascularization is the leading cause of severe visual loss and anti-vascular endothelial growth factor (VEGF) therapy is currently performed for choroidal neovascularization (CNV). Despite its potent anti-angiogenic effect, there are concerns about its long-term safety. Non-steroidal anti-inflammatory drugs (NSAIDs) are common therapeutic agents used for treating inflammatory diseases, and their anti-stress effects are attracting attention now. We studied the effects of topical NSAIDs on CNV, focusing on anti-stress proteins. Cultured retinal pigment epithelium (RPE) cells were treated with NSAIDs: bromfenac, indomethacin, or vehicle control. Transcription factor NF-E2-related factor 2 (Nrf2) and its downstream anti-oxidant protein heme oxygenase (HO)-1 were assessed using western blot and immunohistochemistry. As a result, NSAIDs induced translocation of Nrf2 into the nucleus and the robust expression of HO-1 in a dose- and time-dependent manner. Flow cytometric analysis revealed that bromfenac inhibited H_2O_2-induced apoptosis in cultured RPE cells. Next, we studied the effects of topical bromfenac on laser-induced CNV model in rat. The expressions of Nrf2 and HO-1, infiltrations of ED-1-positive macrophages at CNV lesions and size were analyzed. VEGF in the ocular fluid of these rats was also measured using enzyme-linked immunosorbent assay. Rats administered an inhibitor of HO-1 stannic mesoporphyrin (SnMP) were also studied. The results showed that topical bromfenac led to translocation of Nrf2 and induction of HO-1 in CNV lesions and that the number of infiltrating macrophages at the CNV lesion decreased. The sizes of CNV lesions were significantly smaller in bromfenac-treated rats than control CNV, and the effects were diminished by SnMP. VEGF increased in the ocular fluid after laser treatment and was inhibited by bromfenac and SnMP canceling these effects. NSAIDs inhibit CNV through the novel anti-stress protein HO-1-dependent pathway, indicating its potential therapeutic value for various intraocular angiogenic diseases including CNV.

Laboratory Investigation (2011) **0,** 000–000. doi:10.1038/labinvest.2011.101

KEYWORDS: age-related macular degeneration; anti-VEGF; choroidal atrophy; photodynamic therapy; oxidative stress; steroid

Ocular angiogenesis such as choroidal neovascularization (CNV) is a leading cause of severe vision loss in patients with various ocular diseases.[1–3] Until recently, CNV was not a treatable condition and visual prognosis was poor. However, novel pharmacological therapies such as anti-vascular endothelial growth factor (VEGF) have revolutionized this field.[4,5] Despite significant advances, there are still concerns about the present anti-VEGF treatment. Complete blocking of VEGF is a logically correct method; however, it may induce retinal damage after a long period, because VEGF is a neurotrophic factor and has an important role in the retinal development and neuroprotection.[6,7] There are several reports showing that complete blocking of VEGF results in retinal degeneration in animals.[8,9] Indeed, unexplainable retinal atrophy was noted in some eyes with age-related macular degeneration (AMD) treated after several years of intense anti-VEGF therapy.[10]

Recently, it was reported that non-steroidal anti-inflammatory drugs (NSAIDs) inhibit CNV in animals and a large retrospective study found a reduced incidence of CNV in AMD patients taking aspirin.[11–17] The anti-inflammatory properties of NSAIDs are believed to reside in their ability to inhibit the activity of cyclooxygenase (COX). Indeed COX2 was shown to have a pivotal role in the expression of VEGF in

[1]Department of Ophthalmology, Kagoshima University Graduate School of Medical and Dental Sciences, Kagoshima, Japan; [2]Department of Laboratory and Vascular Medicine, Kagoshima University Graduate School of Medical and Dental Sciences, Kagoshima, Japan and [3]Department of Systems Biology in Thromboregulation, Kagoshima University Graduate School of Medical and Dental Sciences, Kagoshima, Japan
Correspondence: Professor T Sakamoto, MD, PhD, Department of Ophthalmology, Kagoshima University Graduate School of Medical and Dental Sciences, 8-27-1, Sakuragaoka, Kagoshima 890-8520, Japan.
E-mail: tsakamot@m3.kufm.kagoshima-u.ac.jp

Received 17 January 2011; revised 30 March 2011; accepted 28 April 2011

a CNV animal model.[18] However, NSAIDs have other biological actions that inhibit nuclear factor-κB (NF-κB), which has a central role in the expression of various pro-inflammatory mediators.[19] Nonetheless, the real mechanism whereby NSAIDs inhibit CNV is not fully understood.

Heme oxygenase-1 (HO-1) is an anti-stress protein. Not only its substrate, heme, but also various stressors such as oxidative stressors, ultraviolet irradiation, inflammatory cytokines, and heavy metals have been reported to induce HO-1 production.[20–22] HO-1 degrades heme to carbon monoxide (CO), free iron, and biliverdin. Biliverdin is subsequently converted into bilirubin by biliverdin reductase.[20–22] Bilirubin and biliverdin are potent antioxidants, and CO has an anti-apoptotic activity. Therefore, upregulation of HO-1 in cells makes the cells resistant to apoptosis induced by various stressors. It was recently reported that NSAIDs upregulate HO-1 production in some types of cell.[23–27] If this anti-stress effect were inducible with topical NSAIDs, it would be very beneficial to use NSAIDs for the treatment of angiogenesis, because they may inhibit both pathological angiogenesis and potential collateral damage related to treatment. This would be especially advantageous for angiogenic disorders of the central nervous system including CNV. In this study, we explore the influence of NSAIDs on the regulation of anti-stress proteins *in vitro* focusing on their anti-apoptotic action and further on their effects on CNV models *in vivo*.

MATERIALS AND METHODS

Cell Culture

All experiments *in vitro* were performed using ARPE-19, a human diploid retinal pigment epithelium (RPE) cell line, which is in many ways similar to RPE *in vivo* (American Type Culture Collections, Manassas, VA).[28] All cultures were fed twice weekly with Dulbecco's modified Eagle's medium: nutrient mixture F12, plus 10% (vol/vol) fetal bovine serum, 2 mM L-glutamine, and penicillin–streptomycin at 100 IU/ml. Cultures were incubated at 37 °C in 5% (vol/vol) CO_2 incubator and sub-cultured with 0.05% trypsin–EDTA (all products were obtained from Invitrogen-Gibco, Rockville, MD). Subconfluent cultures were trypsinized and seeded for the following experiments.

Western Blot Analysis of NF-E2-Related Factor 2 (Nrf2) and HO-1

ARPE-19 cells were subcultured on 6-cm tissue culture dishes. The cells were serum starved for 3 h and stimulated with the indicated concentration of indomethacine (Funakoshi, Tokyo, Japan), bromfenac (provided from Senju Pharmaceutical, Osaka, Japan) as NSAIDs, or dimethylsulfoxide (DMSO) as control for the indicated time. Nuclear and cytoplasmic extracts of cells were prepared using the Pierce NE-PER nuclear and cytoplasmic extraction kit (Pierce, Rockford, IL). They were subjected to 10% SDS–polyacrylamide gel electrophoresis and transferred to nitrocellulose membranes (GE Healthcare Bio-sciences KK, Piscataway, NJ) as with our previous methods.[28,29] Membranes were incubated with a blocking buffer containing 1% BSA and 5% non-fat milk in 25 mM Tris–HCl-buffered saline with 0.02% Tween 20 (TBST), followed by incubation with the respective primary antibodies (1:200; anti-Nrf2 rabbit polyclonal antibody, 1:500; anti-HO-1 antibody, 1:200; anti-β-actin goat polyclonal antibody, Santa Cruz Biotechnology Inc., CA) in TBST containing 1% non-fat milk overnight at 4°C. After three washes with TBST, membranes were incubated with horseradish peroxidase (HRP)-conjugated anti-rabbit IgG polyclonal antibody (Santa Cruz Biotechnology Inc.) or HRP-conjugated anti-goat IgG polyclonal antibody diluted 1:3000 in TBST containing 2.5% non-fat milk for 1 h. The membrane was washed twice, and immunoreactive bands were visualized using an ECL detection system (GE Healthcare Bio-sciences KK). Immunoreactive bands were quantified and relative sum intensities of bands were compared using Image J Software (US National Institutes of Health).

Immunocytochemistry of Nrf2 and HO-1

Immunocytochemistry was carried out in accordance with our previous method.[28,29] ARPE-19 cells were grown on culture slides and serum starved for 3 h, then treated with the indicated concentration of indomethacin, bromfenac, or DMSO as the control for 3 h. After treatment, slides were washed with PBS, fixed with OptiLyse C (Beckman Coulter, Miami, FL), blocked with 1% BSA in PBS containing 0.1% of triton-X100 (PBST) for 60 min and incubated with polyclonal rabbit anti-Nrf2 and anti-HO-1 antibody (each 1:100; Santa Cruz Biotechnology Inc.) in PBS containing 1.5% BSA for 60 min at room temperature. The slides were washed with PBST, incubated with secondary antibodies, Alexa-Fluor 488-conjugated goat anti-mouse IgG F(ab)2 fragment, and Alexa-Fluor 594-conjugated goat anti-rabbit IgG F(ab)2 fragment (each 1:400; Molecular Probes, Carlsbad, CA) for an additional 60 min in the dark at room temperature. Stained cells were washed, mounted with Shandon Perma-Flour (Thermo Scientific, Waltham, MA), and examined with a Zeiss fluorescence microscope (Zeiss, Oberkochen, Germany).

Flow Cytometric Analysis

To analyze the cellular DNA content, the propidium iodide staining method was used as previously described. Briefly, ARPE-19 cells subcultured on 6-cm dishes at a density of 4.5×10^5 cells per dish and incubated with bromfenac or DMSO as a control were dissolved in medium with 1% fetal bovine serum for 24 h. After treatment for the indicated periods, the cells were washed with PBS. The pellet was resuspended in 70% ethanol (2 ml), and the suspension was incubated at −20 °C for 20 min. Cells were then incubated in the dark for 15 min with propidium iodide (5 g/ml) in PBS in the presence of RNase (5 g/ml). Then, the DNA content was

determined (2×10^4 cells each time) with a FACS analyzer (Epics; Beckman Coulter).

Cell Viability Assay

Cell viability was analyzed from mitochondrial respiratory activity measured using MTT (3-(4,5-dimethylthiazol-2yl)-2,5-diphenol tetrazolium bromide) assay (Wako Chemicals, Osaka, Japan), as described previously.[28] Briefly, 3.5×10^4 ARPE-19 cells were cultured in 24-well plates (500 ml medium per well) and pretreated with 2.5 μM bromfenac or DMSO dissolved in a medium with 1% fetal bovine serum for 24 h. Then, the cells were stimulated with or without hydrogen peroxide (500 μM; Merck, Darmstadt) for 15 min and incubated with MTT (0.5 mg/ml; final concentration) for 3 h. Formazan product was solubilized by the addition of DMSO for 16 h. Dehydrogenase activity was expressed as absorbance at a test wavelength of 570 nm and at a reference wavelength of 630 nm. Assays were performed in triplicate and repeated three times in independent experiments.

Animals

Brown-Norway rats (7 week old male; weight 140–160 g) were purchased from Kyudo (Fukuoka, Japan), and housed in a temperature-controlled room. The animals were kept on a 12-h light–dark schedule and had free access to food and water. All animals were treated in accordance with the ARVO Statement for the Use of Animals in Ophthalmic and Vision Research.

Induction of Experimental CNV

A rat CNV model was made accordance to our previous methods.[30,31] Briefly, rats were anesthetized with a 0.1–0.2 ml of a mixture of 100 mg/ml ketamine and 20 mg/ml xylazine. Pupils were dilated with a topical application of 5.0% phenylephrine and 0.8% tropicamide. CNV was experimentally produced with an argon dye-pulsed laser (Novus Varia, Lumenis, Salt Lake City, UT) and a slit lamp delivery system (SL-130; Carl Zeiss Meditec GmbH, Oberkochen, Germany) at a spot size of 100 μm, duration of 0.05 s, and intensity of 200 mW. Four laser photocoagulations were applied to each eye between the major retinal vessels around the optic disk under the previously described conditions.[30] The morphological end point of the laser injury was the appearance of a cavitation bubble, a sign that is thought to correlate with the disruption of Bruch's membrane. On occasion, the inducing laser burst created an extensive subretinal hemorrhage, and these spots were excluded from any further treatment or analysis.

Evaluation of Effects of Topical Bromfenac on Experimental CNV

A total of 20 male Brown-Norway rats were divided into saline-treated group and bromfenac-treated group. All rats underwent laser photocoagulation of the right eye as described above. Saline-treated group rats received eye drops of saline six times a day for 7 days. Drug administration was started the day after photocoagulation (day 1), and continued until day 7. Bromfenac-treated rats were received eye drops of human use bromfenac ophthalmic solution (Bronuk 0.1% ophthalmic solution, Senju Pharmaceutical) six times a day, for 7 days. The eyes were enucleated on day 8 and subjected to further examinations.

Choroidal Flat Mounts

Rats were anesthetized and perfused with 1 ml PBS containing 50 mg/ml fluorescein-labeled dextran (Sigma Aldrich, St Louis, MO) as previously described elsewhere.[12,13] After the eyes were enucleated and briefly fixed in 4% PFA, the anterior segment was removed and the retina was carefully dissected from the eyecup. Four to six radial cuts were made from the edge to the equator, and the eyecup was flat mounted with the sclera facing down and viewed with a Zeiss fluorescence microscope. Images were captured using the same exposure time for each comparative section, taken with a CCD camera, and the sizes of CNV lesions were measured using Image J.

Western Blot Analysis

Retina–choroid whole mounts were isolated and frozen at −80 °C within 2 min after enucleation. Retina–choroids were later ultrasonically homogenized and cytoplasmic protein extracts were isolated using a Pierce NE-PER nuclear and cytoplasmic extraction kit (Pierce) at 4 °C. The protein extracts (20 μg of protein in each lane) were subjected to the western blot analysis described above. For quantification, blots of five independent experiments were used.

Immunofluorescent Staining

Indirect immunofluorescent staining was carried out as described previously.[28,29] Enucleated eyes from the rats were immediately fixed in 4% paraformaldehyde at 4 °C for 12 h. The anterior segment and the lens were removed, and the remaining eyecup was cytoprotected with 10–30% sucrose in PBS. The eyecups were then frozen in an optimal cutting temperature compound (Sakura Finetech, Tokyo, Japan). Frozen sections (7 μm) were dried and blocked with blocking buffer for 1 h. The antibodies used for staining were rabbit polyclonal anti-Nrf2 antibody, rabbit polyclonal anti-HO-1 antibody (each 1:100; Santa Cruz Biotechnology Inc.), mouse anti-CD68 monoclonal antibody (ED1; 1:800; Serotec, Raleigh, NC), mouse anti-glial fibrillary acidic protein (GFAP) monoclonal antibody (1:400; Sigma Aldrich), mouse anti-RPE 65 monoclonal antibody, and mouse anti-CD31 monoclonal antibody (PECAM-1; 1:250 and 1:100, respectively; Abcam, Cambridge, UK). Normal rabbit or mouse IgG was used instead of primary antibody as a negative control in each case. Secondary antibodies were Alexa-Fluor 488-conjugated goat anti-mouse IgG F(ab)2 fragment and Alexa-Fluor 594-conjugated goat anti-rabbit IgG F(ab)2 fragment (each 1:400; Molecular Probes). Slides were

counterstained with DAPI, mounted with Shandon Perma-Fluor (Thermo Scientific), and viewed with a Zeiss fluorescence microscope. Images were captured using the same exposure time for each comparative section. For all experiments, at least three sections from each eye were evaluated. To quantify the macrophage infiltration, 10 different images were randomly selected by a controller (NY) and examined by masked observers (NA and HO).

Evaluation of Intraocular VEGF

We also measured concentrations of VEGF in the intraocular fluid (mixture of aqueous humor and vitreous fluid) as described previously with some modifications.[30] On day 8, the eyes were enucleated under deep anesthesia, the conjunctival tissue was removed, and the remaining eye tissues (cornea, iris, vitreous body, retina, choroids, and sclera) were collected in a tube and four to six radial cuts were made from the equator to cornea edge and to optic nerve at 4 °C. After centrifugation at 12 000 *g* for 30 s, supernatants were collected, and the concentrations of VEGF were measured using ELISA development kits (R&D Systems, Minneapolis, MN). VEGF concentration was adjusted by each protein concentration as previously described.[29] The adjusted concentration from a single eye was used as the concentration of VEGF.

Statistical Analysis

Because of the skewed distribution, the results were analyzed statistically using nonparametric tests (Mann–Whitney *U*-test) and were expressed as mean and range.

Statistical analyses were performed using SPSS software version 16.0 (SPSS Inc., Chicago, IL). A *P*-value of 0.05 was considered to be statistically significant. To adjust for inflated error resulting from multiple comparisons, the corrected significant *P*-value was defined as 0.05/4 using the Bonferroni correction for multiple comparisons.

RESULTS

NSAIDs Translocated Nrf2 and Upregulated HO-1 in Cultured RPE Cells

First, we examined whether transcriptional factor Nrf2 and phase 2 anti-oxidative protein HO-1 were expressed in ARPE-19 cells. Immunocytochemistry showed Nrf2 was located mainly in the cytoplasm and that HO-1 expression was barely detected in an untreated condition. After treatment with indomethacine or bromfenac, Nrf2 was translocated into the nucleus and HO-1 was abundantly present in the perinuclear lesion and cytoplasm (Figure 1).

Western blot analysis showed that treatment with indomethacine resulted in maximal immunoreactivity against Nrf2 at a concentration of 250 μM and 24 h of treatment, whereas HO-1 showed maximal band at a concentration of 50 μM, and this remained constant at 50–250 μM and showed maximal at 12 h of treatment. Treatment with bromfenac also showed maximal immunoreactivity for Nrf2 at a concentration of 160 μM. HO-1 showed maximal band at 40 μM and remained at 80 μM. Time-course examination showed maximal immunoreactivity at 12 h (Figure 2).

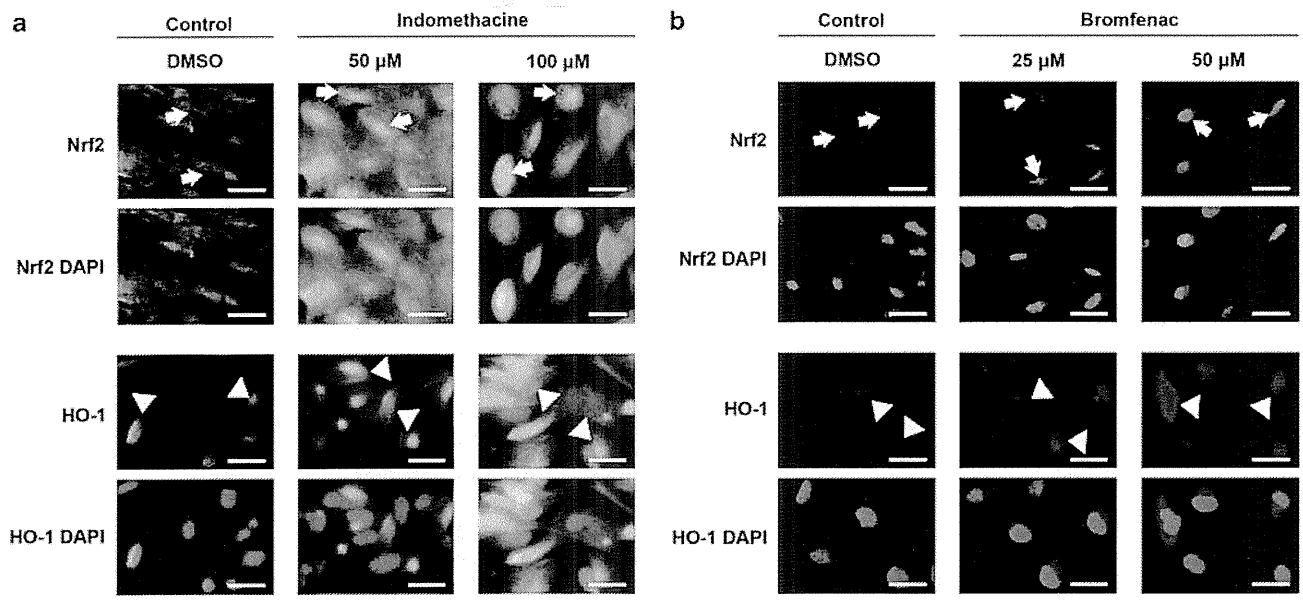

Figure 1 Expressions of Nrf2 and HO-1 protein in immunocytochemistry of ARPE-19 cells. (**a**) Treatment with the indicated concentration of indomethacine upregulated nuclear translocation of Nrf2. Nucleus was translucent or unstained in the control. On the other hand, Nrf2 was upregulated and nucleus is stained after indomethacine treatment (arrows). Cellular expressions of HO-1 were also upregulated in cytosol and nucleus (arrowheads). Scale bars: 30 μm. (**b**) Treatment with bromfenac also showed activation and increased Nrf2 expression in nucleus (arrows). Treatment with bromfenac increased the expression of HO-1 in nucleus and cytosol, especially around nucleus (arrowheads). Scale bars: 30 μm.

Bromfenac Inhibited RPE Cell Apoptosis Caused by Oxidative Stress

It has been reported that HO-1 has an anti-apoptotic property in human gastric mucosal cells.[32] We examined whether HO-1 induced by NSAIDs has functional properties against oxidative stress in ARPE-19 cells. H_2O_2 increased cell apoptosis in either DMSO-treated or bromfenac-treated cells ($15.6 \pm 4.01\%$ to $26.2 \pm 4.22\%$ in DMSO-treated control cells; $P<0.001$ *vs* $15.3 \pm 2.91\%$ to $20.3 \pm 3.02\%$ in bromfenac-treated cells; $P<0.005$). Apoptosis induced by oxidative stress was significantly less in bromfenac-treated cells compared with DMSO-treated control cells ($20.3 \pm 3.02\%$ bromfenac-treated cells *vs* $26.1 \pm 4.22\%$ DMSO-treated cells; $P<0.01$). Treatment with bromfenac itself resulted in no significant difference in apoptosis ($15.6 \pm 4.01\%$ DMSO-treated cells *vs* $15.3 \pm 2.91\%$ bromfenac-treated cells; $P=0.86$; Figure 3a and b).

We also tested cell viability in ARPE-19 cells using MTT assay. As described using propidium iodide staining and a FACS analyzer, H_2O_2 increased cell death of either DMSO-treated or bromfenac-treated cells (0% to $29.0 \pm 2.89\%$ in DMSO-treated control cells; $P<0.001$ *vs* $0.702 \pm 5.73\%$ to $23.5 \pm 4.04\%$ in bromfenac-treated cells; $P<0.001$). Cell death induced by oxidative stress was significantly less in bromfenac-treated cells compared with DMSO-treated control cells ($23.5 \pm 4.04\%$ bromfenac-treated cells *vs* $29.0 \pm 2.89\%$ DMSO-treated cells; $P<0.001$). Treatment with bromfenac itself made no significant difference to cell viability reduction (0% DMSO-treated cells *vs* $0.702 \pm 5.73\%$ bromfenac-treated cells; $P=0.519$;

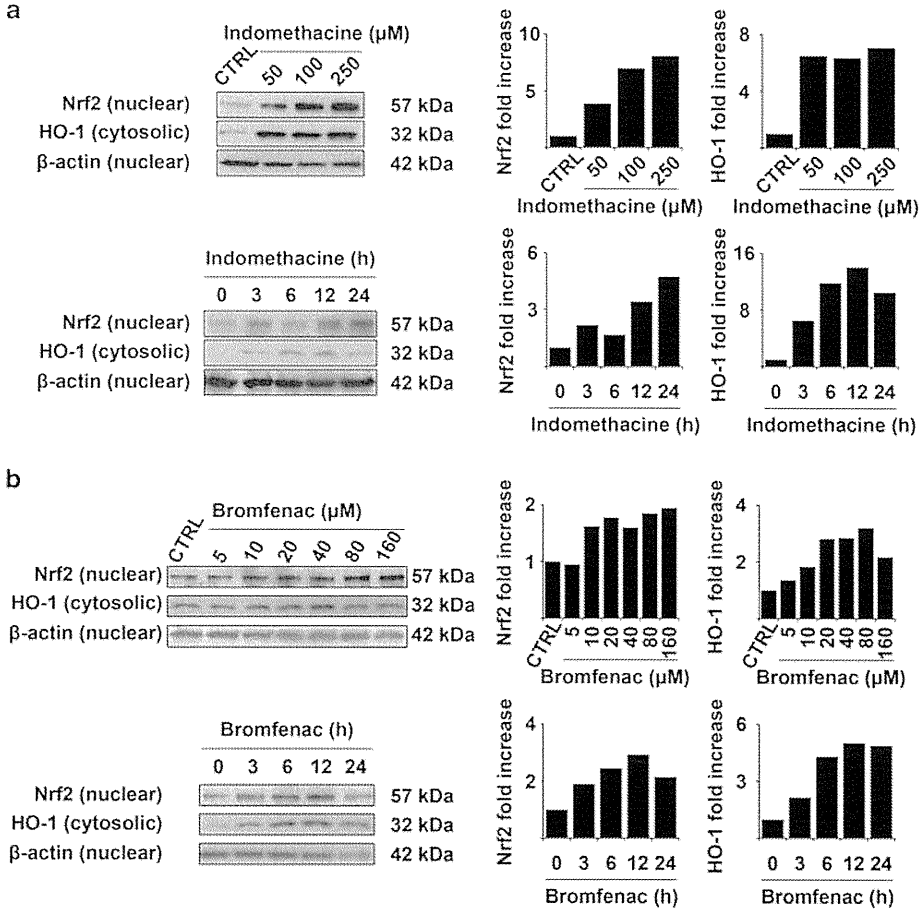

Figure 2 Nrf2 or HO-1 expression in ARPE19 cells by western blot analysis. (**a**; Top row) Serum-starved ARPE-19 cells were stimulated with indomethacine for 3 h and Nrf2 in nuclear protein and HO-1 in cytosolic protein were analyzed using western blots. Nrf2 in nuclear protein was increased by indomethacine in a dose-dependent manner. HO-1 in cytosolic protein is upregulated markedly with 50 μM indomethacine and this trend was continued through stimulation with 250 μM. (Bottom row) ARPE-19 cells were stimulated with indomethacine (250 μM) for the indicated time and subjected to the same analysis. Nrf2 in nuclear protein showed a time-dependent increase. On the other hand, HO-1 in cytosolic protein was showed maximal immunoreactivity at 12 h. (**b**; Top row) ARPE-19 cells were also stimulated with bromfenac for 3 h. Nrf2 was also upregulated in a dose-dependent manner. Increase of HO-1 in cytosolic protein was nearly the same as Nrf2 in nuclear protein. (Bottom row) Time-course expression of Nrf2 in nuclear protein and HO-1 in cytosolic protein with bromfenac (100 μM).

Figure 3c). Statistics were subjected to Mann–Whitney *U*-test with Bonferroni correction.

Reduction of Experimental CNV Size by Bromfenac in Rat Model

Our *in vitro* experiments showed that NSAIDs attenuated H_2O_2-induced RPE cell apoptosis. Next we examined the effects of bromfenac ophthalmic solution in a rat model of CNV. The size of CNV was measured with flat-mounted choroid stained with fluorescein dextran (Figure 4a). As shown in Figure 4b, CNV size was significantly smaller in bromfenac-treated eye ($32\,176 \pm 9165.1\ \mu m^2$) than in saline-treated rats ($48\,383 \pm 12\,733\ \mu m^2$; $P<0.001$, Mann–Whitney *U*-test).

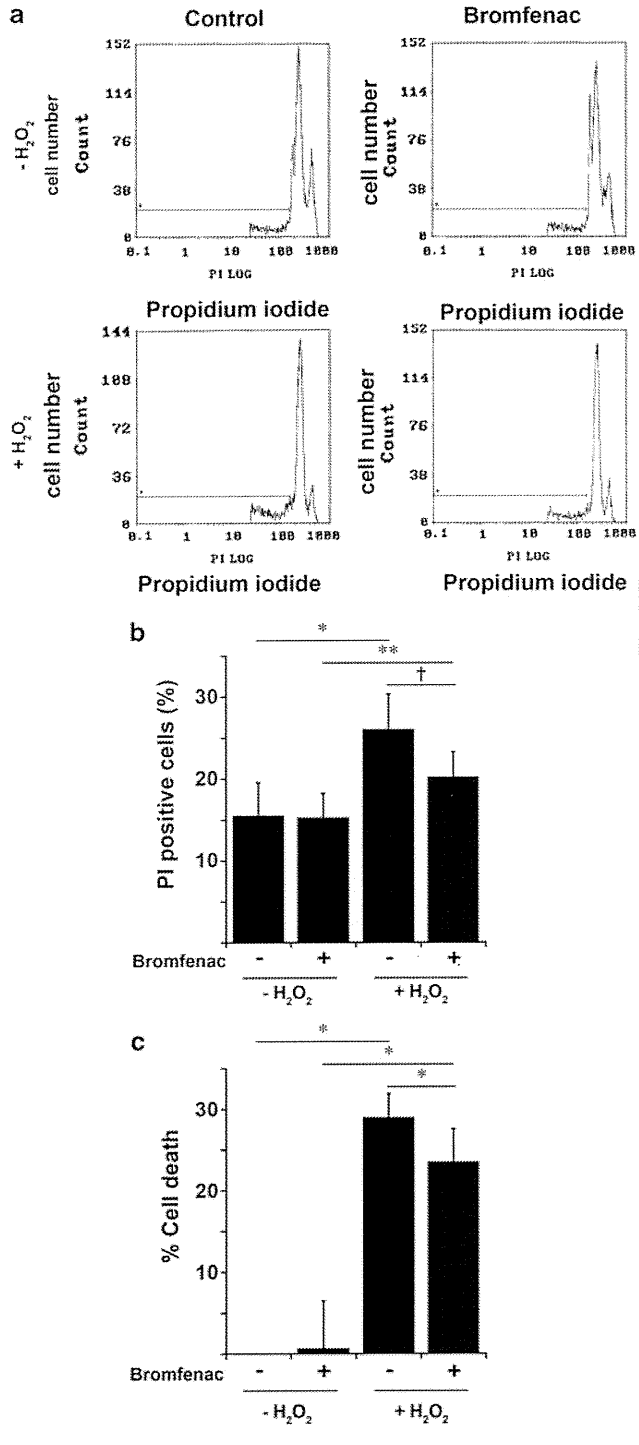

Bromfenac Upregulated Nrf2 and HO-1 in Experimental CNV

The size of experimental CNV was reduced by topical bromfenac. To examine the underlying mechanism, we evaluated expressions of Nrf2 and HO-1 in the CNV area. Our results *in vitro* showed Nrf2 was strongly stained in cell nucleus especially at and adjacent to the CNV area in rats that received bromfenac compared with the control rats. At the same time, expression of HO-1 was observed in cells at CNV lesions. Notably, HO-1 was also strongly found not only at the CNV area but also in the entire retina (Figure 5a and b). To identify the cell type to express HO-1 in bromfenac-treated eyes, the eyes were double stained using anti HO-1 antibody and antibodies specific to each cell type. Anti-RPE65 antibody for RPE cells, anti-GFAP antibody for glial cells, anti-ED1 antibody for macrophages, and anti-CD31 antibody for endothelial cells in the rat CNV model were treated with bromfenac. HO-1 were obviously co-stained with RPE65, GFAP, ED1 antibodies (arrows), implying that RPE cells, GFAP-positive cells (astrocytes or Müller cells), and ED1-positive macrophages were strongly correlated with HO-1 production. HO-1 was also upregulated around

Figure 3 Anti-apoptotic effect of bromfenac was analyzed by flow cytometry. (**a**) ARPE-19 cells were pretreated with bromfenac (left lane) or DMSO (right lane) as a control for 24 h. Then, the cells were stimulated with (bottom) or without (top) 1 mM H_2O_2 for 3 h. After stimulation, the cells were stained with PI, and the DNA content was determined with a FACS analyzer. (**b**) H_2O_2 increased cell apoptosis in both DMSO-treated and bromfenac-treated cells (*$P<0.001$ and **$P<0.005$, respectively). Apoptosis induced by oxidative stress was significantly less in bromfenac-treated cells compared with DMSO-treated control cells ($^{\dagger}P<0.01$). Treatment with bromfenac itself resulted in no significant difference in apoptosis ($P=0.86$). Each group included results of 10 independent examinations ($n=10$). Data were expressed as mean ± s.e.m. The corrected significant *P*-value (Mann–Whitney *U*-test) was defined as 0.0125 (0.05/4 comparisons) after Bonferroni correction. (**c**) Cytoprotective effect of bromfenac was analyzed using MTT assay. ARPE-19 cells were pretreated with bromfenac or DMSO as control for 24 h. Then cells were stimulated with or without 500 μM H_2O_2 for 15 min. After stimulation, cells were incubated with MTT (0.5 mg/ml) for 3 h, formazan product was solubilized by DMSO, dehydrogenase activity was expressed as absorbance and % cell death was determined compared with control. H_2O_2 increased cell death in both DMSO-treated and bromfenac-treated cells (*$P<0.001$). Cell death induced by oxidative stress was significantly less in bromfenac-treated cells compared with DMSO-treated control cells (*$P<0.001$). Treatment with bromfenac itself made no significant difference in cell viability ($P=0.519$). ($n=16$). Data were expressed as mean ± s.e.m. The corrected significant *P*-value (Mann–Whitney *U*-test) was defined as 0.0125 (0.05/4 comparisons) after Bonferroni correction.

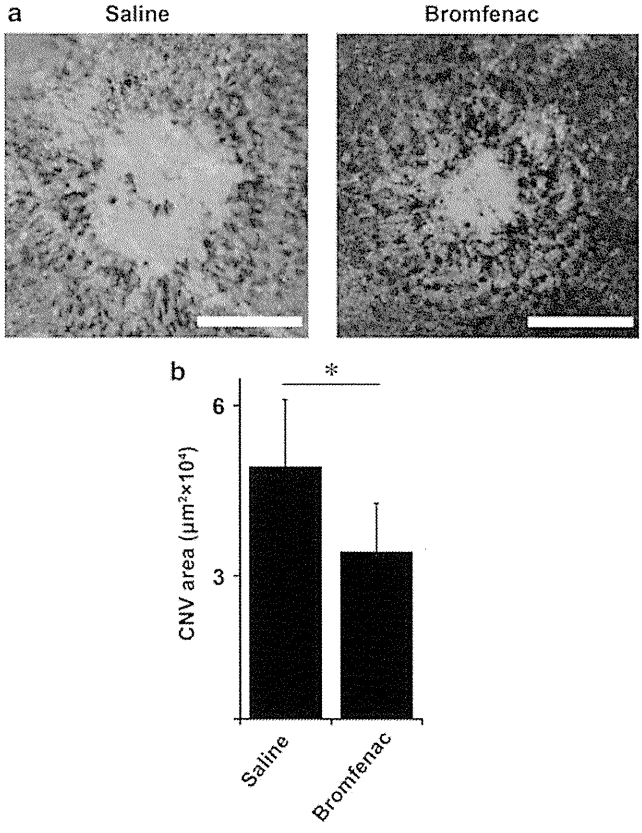

Figure 4 Size of CNV was examined after bromfenac treatment. (**a**) Representative CNV lesions of CNV flat mounts. Scale bars: 200 μm. (**b**) An analysis of the sizes of CNV lesions 8 days after PC. CNV size is smaller in bromfenac eye drop-treated rats 32 176 ± 9165.1 μm^2 than saline eye-drop treated rats 48 383 ± 12 733 μm^2 (*$P<0.001$, Mann–Whitney *U*-test). $n=40$ (40 PC spots of 10 rats). Data were expressed as mean ± s.e.m.

CD31-positive blood vessels, but less co-staining was observed compared with RPE cells or GFAP-positive cells (arrowheads; Figure 5c).

We also examined the protein quantity of Nrf2 and HO-1 using homogenates of retina and choroid of rat CNV model. Western blot analysis showed no immunoreactivity to Nrf2. It is more than probable that the concentration of Nrf2 in the prepared nuclear extract was too low to be detected. Western blot analysis of cytosolic extracts showed that HO-1 was upregulated in the tissue of rat treated with bromfenac as observed in immunohistochemical analysis (Figure 6a). An analysis using densitometry of five independent western blot results confirmed upregulation of HO-1 in bromfenac-treated eyes and photocoagulated (PC) eyes (Figure 6b). Expressions of HO-1 in saline-treated eyes with no PC were defined as base line, and fold increases of HO-1 in other eyes were calculated. Topical bromfenac significantly upregulated HO-1 expression (1.85 ± 0.19-fold, $P<0.01$), and bromfenac-treated eyes with PC expressed more significant HO-1 expression (2.21 ± 0.36-fold, $P<0.01$) compared with saline-treated eyes. Although there was no statistical significance, PC itself slightly upregulated HO-1 expression by 1.21 ± 0.24-fold).

HO-1 Inhibitor Stannic Mesoporphyrin (SnMP) Reversed Inhibitory Effect of Bromfenac on CNV

Upregulation of HO-1 by NSAIDs was observed both in our *in vitro* and *in vivo* experiments. We examined whether the inhibition of HO-1 changed the size of experimental CNV. Topical bromfenac decreased the size of CNV compared with the control (bromfenac rat 28 191 ± 5466 μm^2 *vs* control rat 42 405 ± 9004 μm^2 control: $P<0.001$). This inhibitory effect was diminished by intraperitoneal injection of SnMP (iSnMP; bromfenac rat 28 191 ± 5466 μm^2 *vs* bromfenac + iSnMP rats 44 677 ± 7619 μm^2, $P<0.001$ or control rat 42 405 ± 9004 μm^2 *vs* bromfenac + iSnMP rats 44 677 ± 7619 μm^2, $P=0.923$). On the other hand, iSnMP itself did not have any significant effect on CNV size (44 057 ± 14 775 μm^2; Figure 7).

Inhibitory Effect of Bromfenac on Macrophage Infiltration Was Diminished by SnMP

The above experiments revealed that topical bromfenac reduced the size of the CNV, and iSnMP reversed this reduction (Figure 8). To identify the mechanisms underlying this phenomenon, we measured the number of macrophages infiltrating into the CNV area. As a result, in the group which received intraperitoneal PBS (iPBS), infiltration of macrophage was significantly decreased in bromfenac-treated eyes compared with saline-treated eyes (18.0 ± 6.04 cells/field bromfenac + iPBS rats *vs* 32.4 ± 6.07 cells/field saline + iPBS rats; $P<0.01$). iSnMP reversed this effect and significantly increased macrophage infiltration (18.0 ± 6.04 cells/field bromfenac + iPBS rats *vs* 37.4 ± 4.28 cells/field bromfenac + iSnMP rats; $P<0.01$). There was no significant change with macrophage infiltration in saline-treated rats (31.0 ± 4.24 cells/field saline + iSnMP rats *vs*, 37.4 ± 4.28 cells/field bromfenac + iSnMP rats; $P=0.074$).

Reduction of Intraocular VEGF by Bromfenac Was Diminished by SnMP

The amount of VEGF in ocular fluid obtained from the CNV model on day 8 was evaluated with ELISA. As a result, the amount of VEGF increased in CNV model in comparison with rat eyes without laser burn. VEGF level was significantly lower in bromfenac-treated rat than control CNV rats (1.09 ± 0.88 pg/mg protein bromfena + iPBS rats *vs* 3.08 ± 3.19 pg/mg protein saline + iPBS rats; $P<0.01$). Additional iSnMP increased intraocular VEGF level as high as that of control CNV rats (5.35 ± 4.23 pg/mg protein bromfenac + iSnMP rats *vs* 1.09 ± 0.88 pg/mg protein bromfenac + iPBS rats; $P<0.001$). No significant difference resulted from iSnMP itself (4.09 ± 3.87 pg/mg protein saline + iSnMP rats *vs* 3.08 ± 3.19 pg/mg protein saline + iPBS rats; $P=0.499$; Figure 9).

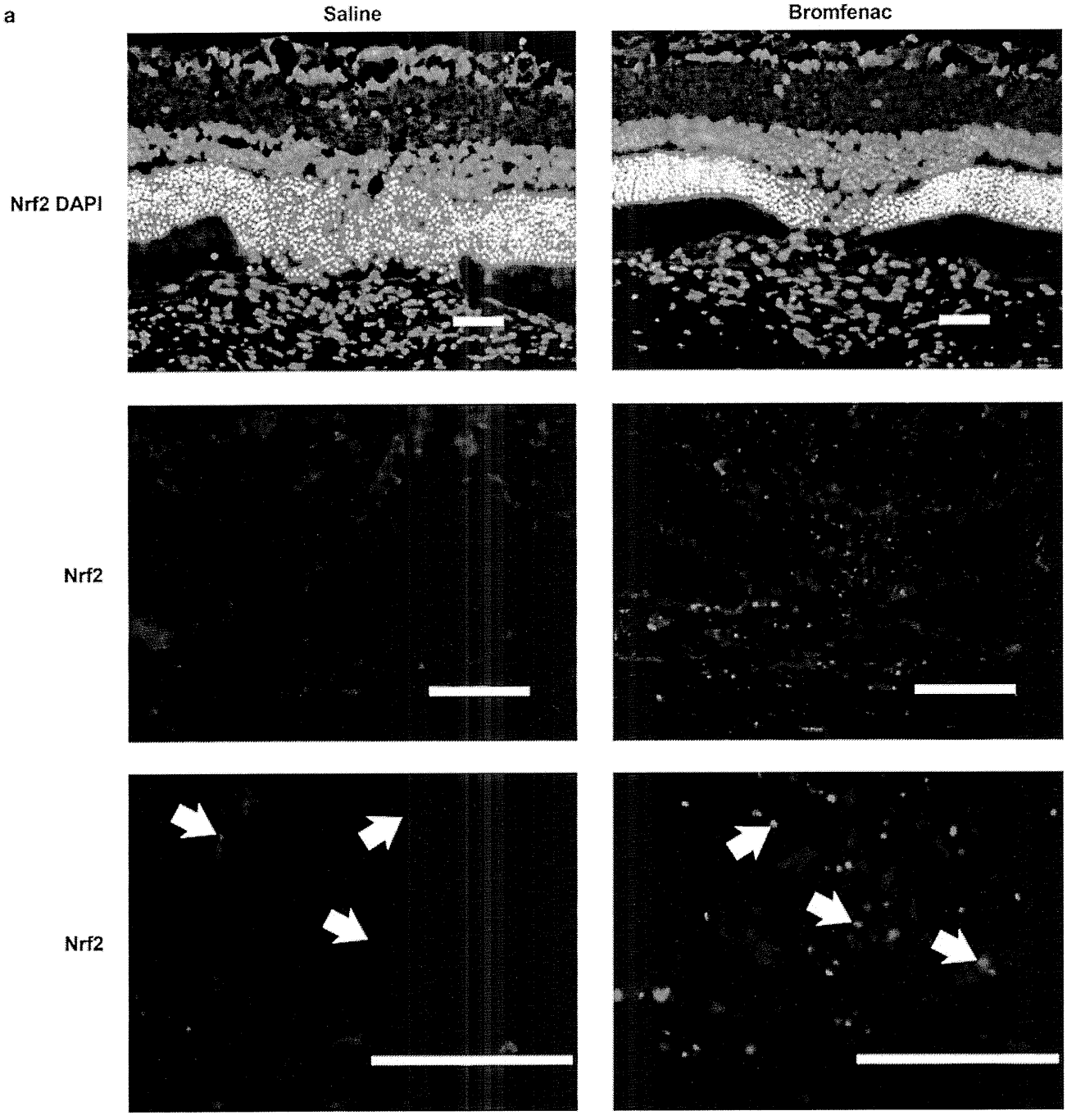

Figure 5 Immunohistochemical analysis was carried out for CNV lesions using Nrf2 or HO-1 protein. Immunofluorescent study was performed with anti-Nrf2 antibody (**a**) and anti-HO-1 antibody (**b**) in rat CNV model. Nuclei were counter-stained with 4′-6-diamidino-2-phenylindole (DAPI). (**a**) The results showed that expression of Nrf2 was upregulated and accumulated in cell nuclear especially at and near the CNV lesion (arrows). (**b**) Expression of HO-1 was also upregulated with bromfenac eye drop compared with saline-treated eye, especially at the photocoagulated CNV area and inner limited membrane (arrowheads). Scale bars: 100 μm. (**c**) Double staining for immunohistochemical analysis with anti-HO-1 antibody and cell-specific antibodies. Anti-RPE65 antibody for RPE cells, anti-GFAP antibody for glial cells, anti-ED1 antibody for macrophages, and anti-CD31 antibody for endothelial cells were in rat CNV model treated with bromfenac. HO-1 were obviously co-stained with RPE65, GFAP, ED1 antibodies (arrows), implying that RPE cells, GFAP-positive cells (astorcytes or Müller cells) and ED1-positive macrophages were strongly correlate with HO-1 production. HO-1 was also upregulated around CD31-positive blood vessels but less co-staining was observed compared with RPE cells or GFAP-positive cells (arrowheads). Nuclei were counter stained with DAPI. Scale bars: 100 μm.

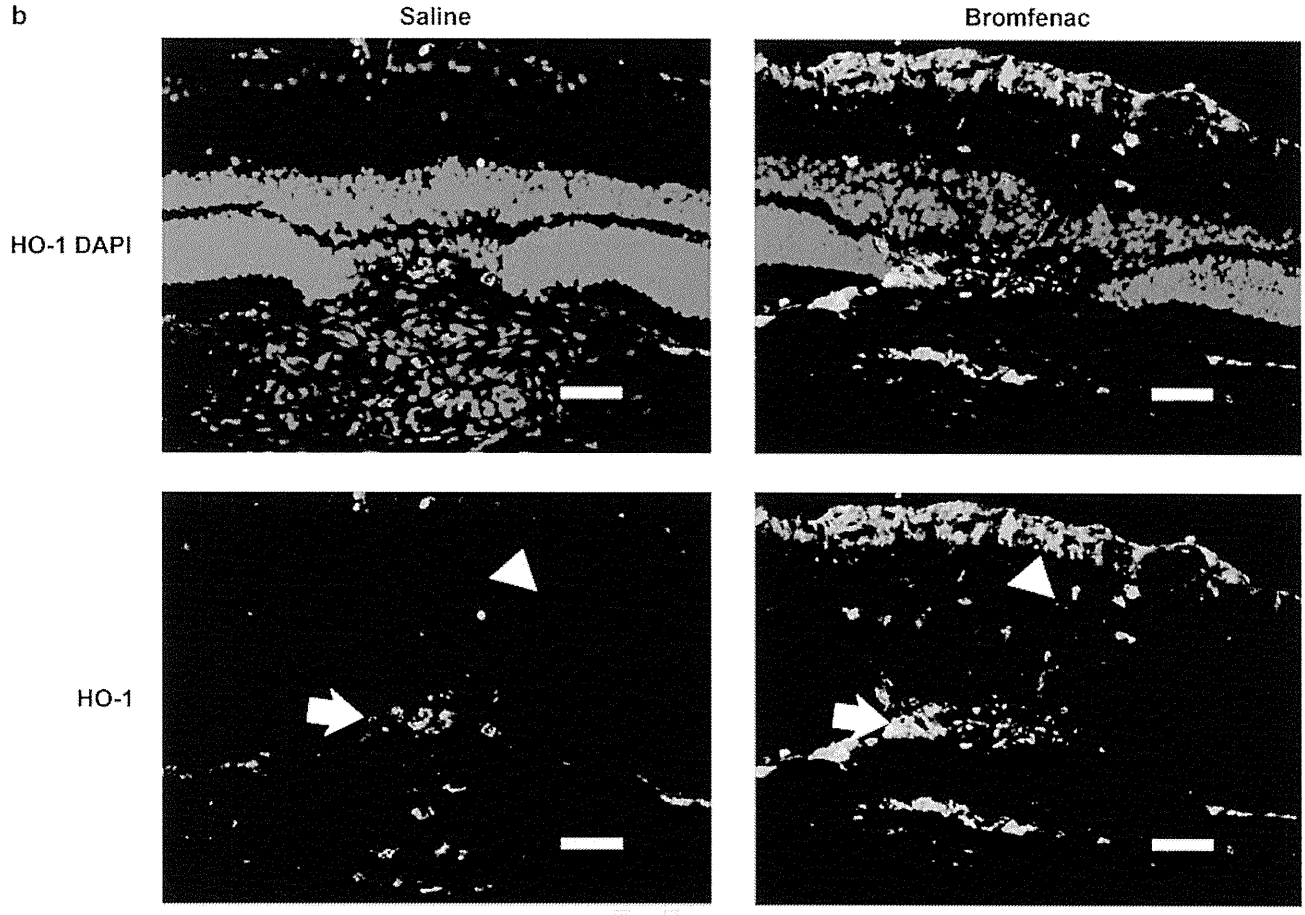

Figure 5 Continued.

DISCUSSION

Previously, we reported that intravitreous NSAIDs inhibited laser-induced CNV in sub-human primate; however, its mechanism was not well addressed.[11] Several recent reports showed possible mechanisms of the inhibitory effect of NSAIDs on CNV.[11–18] VEGF is one of the most potent molecules in angiogenesis. Takahashi *et al*[13] reported that nepafenac inhibited neovascularization in mice with CNV due to laser-induced rupture of Bruch's membrane and Kim *et al*[16] showed that ketrolac reduced the size of laser-induced CNV. Both suggested that the inhibitory effect of NSAIDs was due to downregulation of VEGF expression in the retina. Our previous study showed that blocking VEGF by gene transfer strongly inhibited CNV in this model.[31] Indeed, intraocular VEGF was significantly reduced in bromfenac-treated eyes in this study and thus inhibition of VEGF was also likely to have a crucial role in the inhibition of CNV formation found in this study.

There may be several explanations for the mechanism of this phenomenon. The first is the direct effect of NSAIDs on endothelial cells. It was reported that NSAIDs directly affect endothelial cells to down-regulate VEGF *in vitro*.[33,34] The targeted portions were supposed to be MAP kinase, ERK2 or the expression of VHL tumor suppressor protein, resulting in ubiquitination and degradation of HIF-1α.[33,34] Another report showed that NF-κB, which can also increase the expression of VEGF, and was inhibited by NSAIDs.[35] These direct mechanisms were probably at work in the present model, at least in part. The second is that the present phenomenon was caused by the inhibition of inflammation, which is an indirect effect. This explanation would be quite understandable because inflammatory cells are major sources of VEGF and depletion of macrophage strongly reduced the size of CNV, as demonstrated by ourselves and others.[36] NSAIDs were reported to reduce the prostaglandin, which is a known potent inducer of inflammation, in mouse retina.[14,16] Besides, NF-κB has a central role in the expression of various pro-inflammatory mediators and leukocyte infiltration.[37] So inflammation was inhibited by NSAIDs, consequently reducing the size of CNV. This is compatible with the present result that the number of macrophages infiltrating into the laser burned areas was significantly less in bromfenac-treated eyes than in PBS-treated controls.

In contrast, we shed light on another mechanism of NSAIDs in this study, ie, anti-stress protein in NSAIDs-mediated CNV suppression. Nrf2 is located at the cytosol binding to Keap1 under a stress-free condition; whereas after activation under the stressors, Nrf2 translocates to the

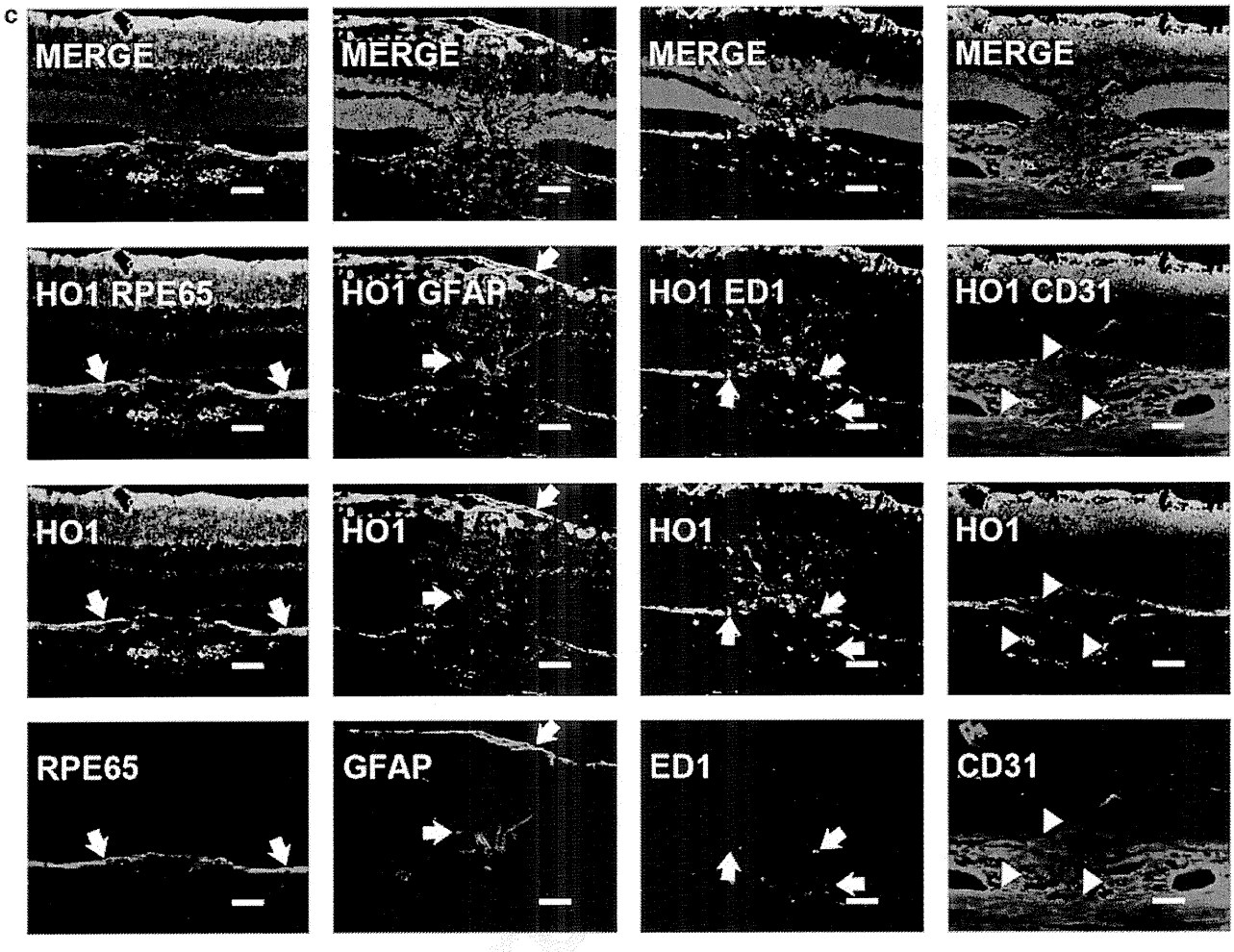

Figure 5 Continued.

nucleus, where it binds to the consensus *cis*-element (Maf-recognition element) to turn on the anti-oxidative stress mechanism, which can result in cell protection.[38,39] Because COX2 inhibits the activity of Nrf2, NSAIDs are supposed to activate the Nrf2/ARE pathways.[39,40] HO-1 is a phase II drug-detoxifying enzyme, such enzymes are regulated in a coordinated manner through a consensus *cis*-element and transcription factors, such as Nrf2. The present findings *in vitro* are consistent with this theory.

To our knowledge, this is the first report to show that NSAIDs induce HO-1 in the retina *in vivo* and *in vitro*. Interestingly, photocoagulation itself increased HO-1 expression in the retina, suggesting that HO-1 was induced by stress such as photocoagulation. However, HO-1 increased in bromfenac-treated eyes with no laser treatment and it was far more significant than in eyes with laser-burn alone. It is noteworthy that the inhibitory effect of bromfenac on CNV was diminished after the administration of SnMP. On the other hand, the size of CNV was not affected by saline eye drops after SnMP administration. These findings suggest that HO-1 does not necessarily have a pivotal role in CNV formation, but has a critical role in the inhibitory processes of bromfenac.

The role of HO-1 in angiogenesis is controversial.[41–43] It is suggested that during inflammation HO-1 has two different roles: first, an anti-inflammatory action inhibiting leukocyte infiltration; and second, promotion of VEGF-driven non-inflammatory angiogenesis, which facilitates tissue repair. In this study, bromfenac increased the expression of HO-1 associated with the inhibition of macrophage infiltration, whereas the inhibition of HO-1 by SnMP significantly augmented macrophage infiltration even in bromfenac-treated eyes. Thus, the increase of HO-1 expression by bromfenac was likely to lead to the inhibition of macrophage infiltration more than the promotion of VEGF-driven non-inflammatory angiogenesis in rat CNV model. Besides, our examination using intraocular fluids revealed that, bromfenac reduced the intraocular VEGF level (Figure 9). Consequently, CNV was inhibited.

Another important impact of HO-1 on retinal cells is its protective role, which was also observed as in the present *in vitro* study. In the *in vivo* study for example, curcumin

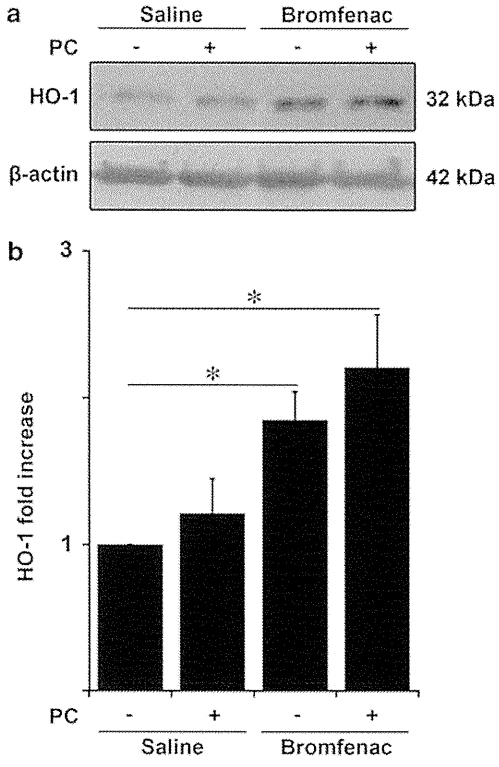

Figure 6 Western blot analysis of HO-1 in cytosolic proteins of rat retina–choroid homogenates. (**a**) Western blot shows HO-1 was upregulated with bromfenac and it was also slightly upregulated in eyes that received photocoagulation (PC) compared with others. (**b**) An analysis using densitometry on five independent western blots confirmed upregulation of HO-1 in bromfenac-treated eyes and photocoagulated eyes. Expressions of HO-1 in saline-treated eyes with no PC were defined as the base line, and fold increases of HO-1 in other eyes were calculated. Topical bromfenac significantly upregulated HO-1 expression ($^*P<0.01$), and bromfenac-treated eyes with PC expressed more significant HO-1 expression ($^*P<0.01$) compared with saline-treated eyes. Although not statistically significant, PC itself slightly upregulated HO-1 expression. The corrected significant *P*-value (Mann–Whitney *U*-test) was defined as 0.0125 (0.05/4 comparisons) after Bonferroni correction. Data were expressed as mean ± s.e.m.

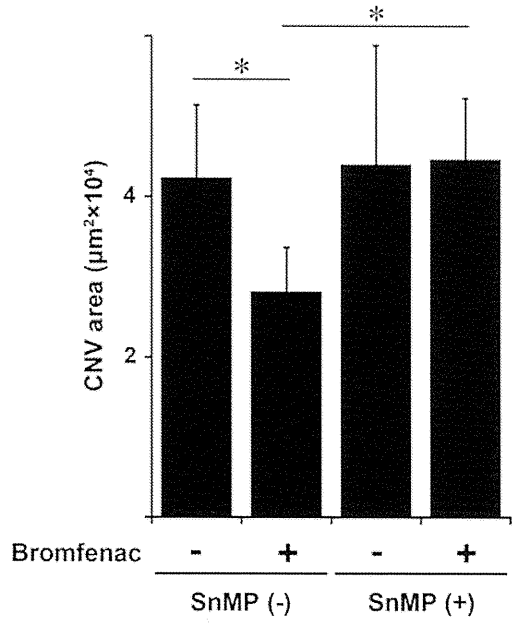

Figure 7 Effects of SnMP on inhibition of bromfenac over CNV size were studied. Topical bromfenac decreased the size of CNV compared with the control (bromfenac rat *vs* control rat. $^*P<0.001$ or bromfenac rat *vs* bromfenac + SnMP rat; $^*P<0.001$). This inhibitory effect was diminished by an inhibitor of HO-1 SnMP (control rat *vs* bromfenac + SnMP rats; $P=0.923$). On the other hand, SnMP itself did not have any significant effect on CNV size. The corrected significant *P*-value (Mann–Whitney *U*-test) was defined as 0.0125 (0.05/4 comparisons) after Bonferroni correction. $n=20$ (PC spots of five rats). Data were expressed as mean ± s.e.m.

protects retinal cells from light- or oxidant stress-induced cell death through the induction of HO-1.[44] Overexpression of HO-1 by gene transfer also inhibited light-induced photoreceptor cell apoptosis through Bcl-2 upregulation.[45] There are other reports showing that the induction of HO-1 by various stimulants rescued the retina in an ischemia-reperfusion model.[46] Therefore, NSAIDs might be beneficial for the treatment of CNV beyond their anti-angiogenic effect. This is especially true for the treatment of diseases of central nervous tissue including eye. At present, regeneration of neural tissue is clinically still difficult. Even if angiogenesis were to be blocked by an anti-VEGF drug, it would not necessarily mean the tissue function is protected. We need a potent angiogenesis therapy, but it must protect the host tissue as well. NSAIDs might be reasonable candidate drugs for this purpose.

It should be noted that there are other mechanisms to protect the retina from oxidative stress. Qin *et al*[47] showed that cyclopentenone 15-deoxy-delta^{12,14}-prostaglandin J2 protects RPE cells from oxidative injury. Although this mechanism is not evaluated in the present study, it is highly probable that these factors as a whole resulted in the present phenomenon.

There are different kinds of NSAIDs available. Each has different characteristics related to ocular penetration and inhibitory activity of COXs. For example, topical administration of 0.1% nepafenac inhibits the synthesis of PGs in the retina–choroid by 55% for 4 h.[48] Although, topical bromfenac has good ocular penetration and reaches a sufficient level in the retina and choroid, the inhibitory activity of bromfenac on either COX-1 or COX-2 was stronger than nepafenac or dicrofenac.[49,50] In our pilot study, we tested several different NSAIDs and found that topical bromfenac had a sufficient inhibitory effect on CNV in rat, as expected. Therefore, we chose bromfenac for the present study. But, it should be noted that the present results can be applied to bromfenac.

The present study has limitations. The present CNV model does not perfectly reflect clinical conditions. Certainly AMD or high myopia is a chronic and long-lasting disease. On the other hand, the present model is an acute wound-healing

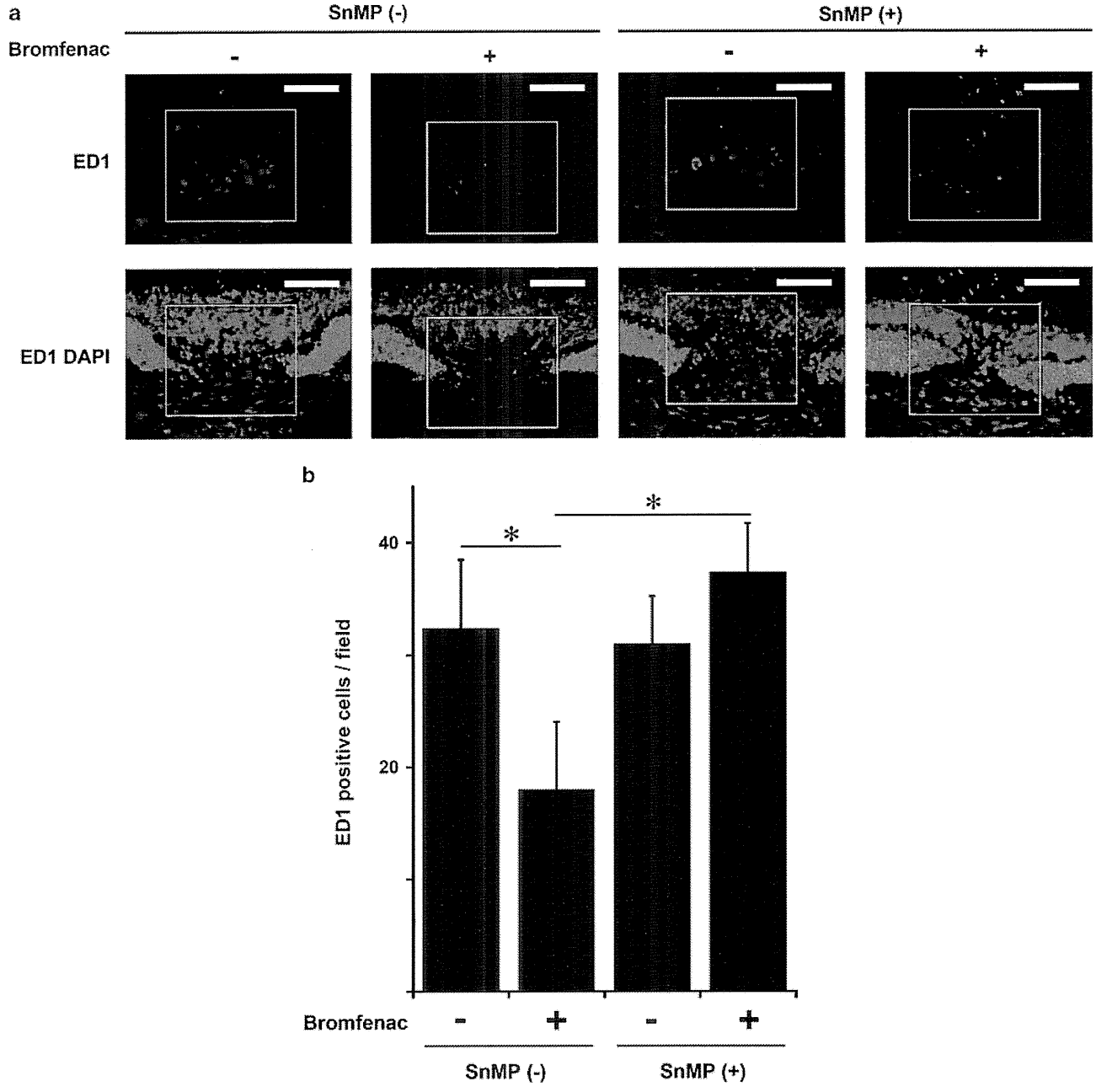

Figure 8 The number of infiltrating ED1-positive macrophages in CNV lesions was examined. (**a**) Representative images of rat CNV lesion identified by immunofluorescence with anti-ED1 antibody (red) and DAPI (blue). Scale bars: 150 μm (**b**). The number of ED1-positive macrophage infiltration expressed mean ± s.e.m. cells/field. In the group that received intraperitoneal PBS, infiltration of macrophage was decreased more significantly in bromfenac-treated rats than saline-treated rats (*$P<0.01$). Intraperitoneal injections of SnMP reversed this effect and significantly increased macrophage infiltration (*$P<0.01$). There was no significant change with macrophage infiltration in saline eye drop-treated rats ($P=0.074$). $n=10$. The corrected significant *P*-value (Mann–Whitney *U*-test) was defined as 0.0125 after Bonferroni correction. Square indicates CNV lesion.

model rather than a chronic disease model. Nonetheless, CNV in humans occurs in a similar manner to angiogenesis processes in acute wound healing and the present results will help an understanding of the clinical CNV. The second is that we measured the protein level of HO-1, but not its activity. The amount of protein does not necessarily reflect its biological activity. But the fact that an inhibitor of HO-1 reversed the effects of bromfenac indicates that HO-1 is likely to have played a major role in inhibiting CNV by bromfenac. The third is the treatment efficacy of NSAIDs. The current intravitreous anti-VEGF therapy is so potent for inhibiting CNV that there may be concerns that any new treatment will hardly improve on the current anti-VEGF therapy. However, complete blocking of VEGF might be potentially harmful

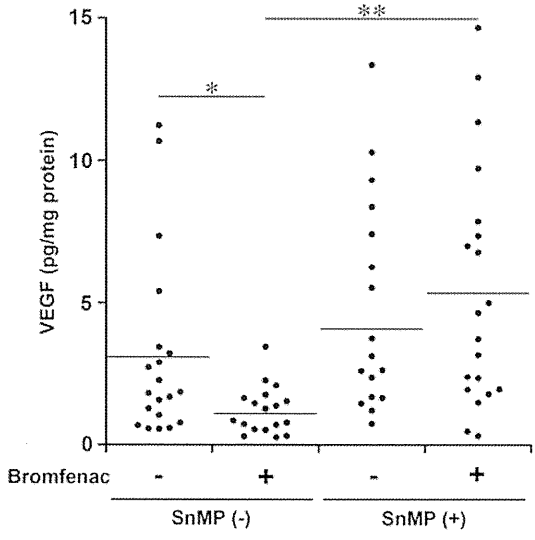

Figure 9 VEGF level of intraocular fluid in each eye was plotted. Analysis of intraocular fluid using ELISA showed that intraocular VEGF level was lower in bromfenac-treated rat (*$P<0.01$). Additional injection of SnMP increased intraocular VEGF level as high as in control CNV rats (**$P<0.001$). No significant difference resulted from intraperitoneal SnMP alone. Each group contained 20 samples from 20 eyes ($n=20$). Mean value of each group was expressed by a line. The corrected significant *P*-value (Mann–Whitney *U*-test) was defined as 0.0125 after Bonferroni correction.

after a long period.[7,10] Topical NSAIDs had therapeutic effects on CNV in this study. Because it has such a potentially neuroprotective effect, combination therapy with an anti-VEGF drug may be very advantageous for patients. Combination therapy is found to be more effective, but is less likely to result in drug resistance than mono-therapy in the t reatment of tumor angiogenesis.[51] In addition, repeated intravitreal injections were necessary for the majority of patients to maintain this level of benefit.[4,5] Intravitreal injections can be physically uncomfortable, and they expose the patient to a number of potential vision-threatening complications such as intraocular infection. Topical administration of a drug that has the capacity to substantially reduce CNV would be a promising advance in the development of therapies for neovascular eye diseases. Finally, there was a technical problem in this study. RT-PCR might be more suitable for objective quantification of invading macrophages. We performed RT-PCR using a primer for macrophage; however, no reproducible data were obtained (data not shown). The results were strongly affected by the size of photocoagulation spot or sampling biases. This limitation should be also noted.

In conclusion, the present study showed a new mechanism of NSAIDs for inhibiting neovascularization of the choroid. Topical NSAIDs would be beneficial for the treatment of CNV not only because of its anti-angiogenic effect but also its potential anti-stress effect. Because the CNV model can be a mirror for other angiogenic diseases in the central nervous system, NSAIDs could be studied more widely and profoundly as a candidate therapy for these disease conditions (Supplementary Figure 1). Q4

Supplementary Information accompanies the paper on the Laboratory Investigation website (http://www.laboratoryinvestigation.org)

ACKNOWLEDGEMENTS

This work was supported by a grant from the Research Committee on Chorioretinal Degeneration and Optic Atrophy, Ministry of Health, Labor, and Welfare, Tokyo, Japan; and by a Grant-in-Aid for Scientific Research from the Ministry of Education, Science, and Culture of the Japanese Government, Tokyo, Japan.

DISCLOSURE/CONFLICT OF INTEREST

The authors declare no conflict of interest.

1. Bressler NM, Bressler SB, Fine SL. Age-related macular degeneration. Surv Ophthalmol 1988;32:375–413.
2. Soubrane G. Choroidal neovascularization in pathologic myopia: recent developments in diagnosis and treatment. Surv Ophthalmol 2008;53:121–138.
3. Cohen SY, Laroche A, Leguen Y, *et al.* Etiology of choroidal neovascularization in young patients. Ophthalmology 1996;103: 1241–1244.
4. TAP study group. Photodynamic therapy of subfoveal choroidal neovascularization in age-related macular degeneration with verteporfin: one-year results of 2 randomized clinical trials–TAP report. Treatment of age-related macular degeneration with photodynamic therapy (TAP) Study Group. Arch Ophthalmol 1999;117:1329–1345.
5. Rosenfeld PJ, Brown DM, Heier JS, *et al.* Ranibizumab for neovascular age-related macular degeneration. N Engl J Med 2006;355:1419–1431.
6. Nishijima K, Ng YS, Zhong L, *et al.* Vascular endothelial growth factor-A is a survival factor for retinal neurons and a critical neuroprotectant during the adaptive response to ischemic injury. Am J Pathol 2007;171:53–67.
7. Robinson GS, Ju M, Shih SC, *et al.* Nonvascular role for VEGF: VEGFR-1, 2 activity is critical for neural retinal development. FASEB J 2001;15:1215–1217.
8. Murakami Y, Ikeda Y, Yonemitsu Y, *et al.* Inhibition of choroidal neovascularization via brief subretinal exposure to a newly developed lentiviral vector pseudotyped with Sendai viral envelope proteins. Hum Gene Ther 2010;21:199–209.
9. Saint-Geniez M, Kurihara T, Sekiyama E, *et al.* An essential role for RPE-derived soluble VEGF in the maintenance of the choriocapillaris. Proc Natl Acad Sci USA 2009;106:18751–18756.
10. Rosenfeld PJ, Shapiro H, Tuomi L, *et al.* Characteristics of patients losing vision after 2 years of monthly dosing in the phase III ranibizumab clinical trials. Ophthalmology 2011;118:523–530.
11. Sakamoto T, Soriana D, Nassaralla J, *et al.* Effect of intravitreal administration of indomethacin on experimental subretinal neovascularization in the subhuman primate. Arch Ophthalmol 1995; 113:222–226.
12. Takahashi H, Yanagi Y, Tamaki Y, *et al.* COX-2-selective inhibitor, etodolac, suppresses choroidal neovascularization in a mice model. Biochem Biophys Res Commun 2004;325:461–466.
13. Takahashi K, Saishin Y, Saishin Y, *et al.* Topical nepafenac inhibits ocular neovascularization. Invest Ophthalmol Vis Sci 2003;44:409–415.
14. Yanni SE, Clark ML, Yang R, *et al.* The effects of nepafenac and amfenac on retinal angiogenesis. Brain Res Bull 2010;81:310–319.
15. Kim SJ, Toma HS. Inhibition of choroidal neovascularization by intravitreal ketorolac. Arch of Ophthalmol 2010;128:596–600.
16. Kim SJ, Toma HS, Barnett JM, Penn JS. Ketorolac inhibits choroidal neovascularization by suppression of retinal VEGF. Exp Eye Res 2010;91:537–543.
17. Wilson HL, Schwartz DM, Bhatt HR, *et al.* Statin and aspirin therapy are associated with decreased rates of choroidal neovascularization among patients with age-related macular degeneration. Am J Ophthalmol 2004;137:615–624.

18. Rezaei KA, Toma H, Cai J, *et al.* Reduced choroidal neovascular membrane formation in cyclooxygenase-2 null mice. Invest Ophthalmol Vis Sci 2010;52:701–707.
19. Tegeder I, Pfeilschifter J, Geisslinger G. Cyclooxygenase-independent actions of cyclooxygenase inhibitors. FASEB J 2001;15:2057–2072.
20. Ponka P. Cell biology of heme. Am J Med Sci 1999;318:241–256.
21. Maines MD. The heme oxygenase system: a regulator of second messenger gases. Annu Rev Pharmacol Toxicol 1997;37:517–554.
22. Brouard S, Otterbein LE, Anrather J, *et al.* Carbon monoxide generated by heme oxygenase 1 suppresses endothelial cell apoptosis. J Exp Med 2000;192:1015–1026.
23. Alcaraz MJ, Habib A, Créminon C, *et al.* Heme oxygenase-1 induction by nitric oxide in RAW 264.7 macrophages is upregulated by a cyclo-oxygenase-2 inhibitor. Biochim Biophys Acta 2001;1526:13–16.
24. Hou CC, Hung SL, Kao SH, *et al.* Celecoxib induces heme-oxygenase expression in glomerular mesangial cells. Ann NY Acad Sci 2005; 1042:235–245.
25. Nascimento-Silva V, Arruda MA, Barja-Fidalgo C, *et al.* Novel lipid mediator aspirin-triggered lipoxin A4 induces heme oxygenase-1 in endothelial cells. Am J Physiol Cell Physiol 2005;289:C557–C563.
26. Grosser N, Abate A, Oberle S, *et al.* Heme oxygenase-1 induction may explain the antioxidant profile of aspirin. Biochem Biophys Res Commun 2003;308:956–960.
27. Cantoni L, Valaperta R, Ponsoda X, *et al.* Induction of hepatic heme oxygenase-1 by diclofenac in rodents: role of oxidative stress and cytochrome P-450 activity. J Hepatol 2003;38:776–783.
28. Arimura N, Ki-i Y, Hashiguchi T, *et al.* Intraocular expression and release of high-mobility group box 1 protein in retinal detachment. Lab Invest 2009;89:278–289.
29. Otsuka H, Arimura N, Sonoda S, *et al.* Stromal cell-derived factor-1 is essential for photoreceptor cell protection in retinal detachment. Am J Pathol 2010;177:2268–2277.
30. Fujimoto T, Sonoda KH. Choroidal neovascularization enhanced by Chlamydia pneumoniae via Toll-like receptor 2 in the retinal pigment epithelium. Invest Ophthalmol Vis Sci 2010;51:4694–4702.
31. Honda M, Sakamoto T, Ishibashi T, *et al.* Experimental subretinal neovascularization is inhibited by adenovirus-mediated soluble VEGF/flt-1 receptor gene transfection: a role of VEGF and possible treatment for SRN in age-related macular degeneration. Gene Ther 2000;7:978–985.
32. Aburaya M, Tanaka K-I, Hoshino T, *et al.* Heme oxygenase-1 protects gastric mucosal cells against non-steroidal anti-inflammatory drugs. J Biol Chem 2006;281:33422–33432.
33. Jones MK, Wang H, Peskar BM, *et al.* Inhibition of angiogenesis by nonsteroidal anti-inflammatory drugs: insight into mechanisms and implications for cancer growth and ulcer healing. Nat Med 1999;5: 1418–1423.
34. Jones MK, Szabó IL, Kawanaka H, *et al.* von Hippel Lindau tumor suppressor and HIF-1alpha: new targets of NSAIDs inhibition of hypoxia-induced angiogenesis. FASEB J 2002;16:264–266.
35. Ferrara N. Vascular endothelial growth factor and the regulation of angiogenesis. Recent Prog Horm Res 2000;55:15–35.
36. Tsutsumi C, Sonoda KH, Egashira K, *et al.* The critical role of ocular-infiltrating macrophages in the development of choroidal neovascularization. J Leukoc Biol 2003;74:25–32.
37. Ghosh S, May MJ, Kopp EB. NF-kappa B and Rel proteins: evolutionarily conserved mediators of immune responses. Annu Rev Immunol 1998;16:225–260.
38. Jaiswal AK. Nrf2 signaling in coordinated activation of activation of antioxidant gene expression. Free Radic Biol Med 2004;36: 1199–1207.
39. Kaspar JW, Niture SK, Jaiswal AK. Nrf2:INrf2 (Keap1) signaling in oxidative stress. Free Radic Biol Med 2009;47:1304–1309.
40. Healy ZR, Lee NH, Gao X, *et al.* Divergent responses of chondrocytes and endothelial cells to shear stress: cross-talk among COX-2, the phase 2 response, and apoptosis. Proc Natl Acad Sci USA 2005;102: 14010–14015.
41. Bussolati B, Ahmed A, Pemberton H, *et al.* Bifunctional role for VEGF-induced heme oxygenase-1 *in vivo*: induction of angiogenesis and inhibition of leukocytic infiltration. Blood 2004;103:761–766.
42. Dulak J, Loboda A, Zagórska A, Józkowicz A. Complex role of heme oxygenase-1 in angiogenesis. Antioxid Redox Signal 2004;6: 858–866.
43. Bussolati B, Mason JC. Dual role of VEGF-induced heme-oxygenase-1 in angiogenesis. Antioxid Redox Signal 2006;8:1153–1163.
44. Mandal MN, Patlolla JM, Zheng L, *et al.* Curcumin protects retinal cells from light-and oxidant stress-induced cell death. Free Radic Biol Med 2009;46:672–679.
45. Shyong MP, Lee FL, Hen WH, *et al.* Viral delivery of heme oxygenase-1 attenuates photoreceptor apoptosis in an experimental model of retinal detachment. Vision Res 2008;48:2394–2402.
46. Sun MH, Su Pang JH, Chen SL, *et al.* Retinal protection from acute glaucoma-induced ischemia-reperfusion injury through pharmacological induction of heme oxygenase-1 by cobalt protoporphyrin. Invest Ophthalmol Vis Sci 2010;51:4798–4808.
47. Qin S, McLaughlin AP, De Vries GW. Protection of RPE cells from oxidative injury by 15-deoxy-delta12,14-prostaglandin J2 by augmenting GSH and activating MAPK. Invest Ophthalmol Vis Sci 2006;47: 5098–5105.
48. Gamache DA, Graff G, Brady MT, *et al.* Nepafenac, a unique non-steroidal prodrug with potential utility in the treatment of trauma-induced ocular inflammation. I: assessment of anti-inflammatory efficacy. Inflammation 2000;24:357–370.
49. Isaka M, Inada K, Tsutsumi S, *et al.* Ocular tissue distribution in rabbit after instillation of bromfenac sodium ophthalmic solution. Drug Metabol Pharmacokinet 1999;14:32–41.
50. Kida T, Ogawa T, McNamara TR, *et al.* Evaluations of the human COX-1 and COX-2 inhibition for amfenac, bromfenac, ciclofenac, and ketorolac. Annu Meet Guide Abstr Am Coll Clin Pharm 2007; (Suppl):274.
51. Abdollahi A, Folkman J. Evading tumor evasion: current concepts and perspectives of anti-angiogenic cancer therapy. Drug Resist Updat 2010;13:16–28.

Q5

Autofluorescence of the Cells in Human Subretinal Fluid

Tetsuju Sekiryu,[1] *Yasuharu Oguchi,*[1] *Seisuke Arai,*[2] *Ikuo Wada,*[2] *and Tomohiro Iida*[1]

Purpose. The origin of autofluorescence in the subretinal space and the autofluorescence properties of the cells were investigated in surgically collected subretinal fluid.

Methods. Subretinal fluid was surgically collected from four eyes of patients with rhegmatogenous retinal detachment (three eyes) and Coats' disease (one eye). After cytocentrifuge preparation of the cells in the fluid and immunofluorescence staining, a cytologic examination was conducted by using confocal scanning laser microscopy. The autofluorescence of the cells was elucidated by measuring the fluorescence spectra with spectroscopy, to obtain different excitation laser light emission fingerprints.

Results. The cells from the subretinal fluid were classified into three types: CD68-negative cells containing numerous pigmented granules, CD68-positive cells containing few pigments, and CD68-negative cells with no pigmented granules. Autofluorescence was observed in the inclusions of the cells classified into the former two types. When the cells were excited by a 458- or 488-nm laser light, emission spectra in autofluorescence showed little difference between CD68-positive and -negative cells. Peak analysis confirmed that the two types of cells showed the same emission peaks within this range of excitation light.

Conclusions. Autofluorescent inclusions appeared in the CD68-positive and -negative cells in the subretinal fluid. The macrophages in the subretinal fluid possess autofluorescence that is spectroscopically similar to lipofuscin. Autofluorescence of macrophages can be attributed to degenerated outer segments and debris from apoptotic photoreceptors. Clinicians should consider migration of macrophages, in addition to retinal pigment epithelium, as the possible source when abnormal fundus autofluorescence is observed using an ordinary set of fluorescence filters. (*Invest Ophthalmol Vis Sci.* 2011;52: 8534–8541) DOI:10.1167/iovs.11-8012

Fundus autofluorescence (FAF) mainly originates from lipofuscin in the retinal pigment epithelium. Recent studies revealed that a main constituent of lipofuscin that generates autofluorescence is pyridinium bisretinoid (A2E).[1–3] The derivatives of A2E in the photoreceptor outer segments are considered to be another source of abnormal FAF. Novel imaging technology of FAF and optical coherence tomography demonstrated subretinal autofluorescent deposits in some macular diseases with serous retinal detachment, such as vitelliform macular dystrophy,[4,5] central serous chorioretinopathy,[6–11] choroidal melanoma,[12] and Vogt-Koyanagi-Harada disease.[13] Various materials or cells have been proposed as the origin of autofluorescent deposits. These include migrating retinal pigment epithelial cells, debris of degenerated photoreceptor outer segments, or macrophages that have phagocytosed the outer segments. Among them, macrophages are thought to be the main source of the subretinal autofluorescent deposits.[14] Migrating macrophages in the subretinal space are often found in histopathologic specimens and surgically excised tissue from patients with several retinal diseases, such as Best's vitelliform macular dystrophy,[15,16] age-related macular degeneration,[17,18] macular holes,[19] rhegmatogenous retinal detachment (RRD),[20,21] and Coats' disease.[21,22] However, it is not clearly demonstrated that macrophages are the source of autofluorescence in the subretinal space. In the present study, we investigated surgically collected cells in the subretinal fluid and characterized the fluorescence properties of the cells.

Methods

This study complied with the Declaration of Helsinki. The institutional review board at Fukushima Medical University School of Medicine approved: (1) observation using optical coherence tomography and FAF in eyes with macular and retinal disorders and the retrospective comparative analysis performed in this study and (2) biochemical or histopathologic examination of tissues and fluid collected from the eyes at the time of surgery. Written informed consent was obtained from all patients.

Subretinal fluid from four eyes of four patients who had retinal detachment was examined. All four eyes showed hyperautofluorescence in the area of retinal detachment. Three eyes with long-standing RRD and one eye with Coats' disease underwent a routine ophthalmic examination, including determination of best corrected visual acuity (BCVA), intraocular pressure, slit lamp biomicroscopy with a contact lens, and fundus color photography. Fundus autofluorescence was taken with a confocal laser scanning ophthalmoscope (HRA2; Heidelberg Engineering, Heidelberg, Germany) using 488-nm excitation laser and a barrier filter at 500 nm.

Fluid Collection

Subretinal fluid was collected during surgery for retinal detachment. All three eyes with RRD were treated with a scleral buckling procedure. The subretinal fluid was aspirated with a blunt needle attached to a sterilized syringe and introduced into the site of scleral puncture for subretinal fluid drainage. The cryopexy was always performed after subretinal fluid drainage. Specimens with blood contamination were discarded. The eye with Coats' disease was treated with vitrectomy. After aspiration of the crystalline lens and core vitrectomy, an intentional tear was made in the upper temporal quadrant by intraocular diathermy. During fluid–air exchange for retinal reattachment, the subretinal fluid was passively aspirated from the intentional tear into a sterilized syringe. Retinal photocoagulation around the intentional tear and the area of retinal vascular abnormality was made after reattachment of the retina. All four eyes were reattached after a single surgery.

From the Departments of [1]Ophthalmology and [2]Cell Science, Fukushima Medical University School of Medicine, Fukushima, Japan.

Submitted for publication June 9, 2011; revised August 23 and September 21, 2011; accepted September 21, 2011.

Disclosure: **T. Sekiryu**, None; **Y. Oguchi**, None; **S. Arai**, None; **I. Wada**, None; **T. Iida**, None

Corresponding author: Tetsuju Sekiryu, Department of Ophthalmology, Fukushima Medical University School of Medicine, 1 Hikarigaoka, Fukushima City, Fukushima, 960-1295, Japan; sekiryu@fmu.ac.jp.

Investigative Ophthalmology & Visual Science, October 2011, Vol. 52, No. 11

TABLE 1. Clinical Features of the Patients

Patient	Age	Sex	Disease	Subretinal Deposits	Subretinal Strand	Duration of Retinal Detachment	FAF
Patient 1	11	Male	RRD	+	+	unknown	Granular
Patient 2	17	Male	RRD	+	+	4.5M	Granular
Patient 3	24	Male	RRD	+	+	6M	Granular
Patient 4	15	Male	Coats' disease	+	+	4M	Diffuse

Fluorescence Spectroscopy

Collected subretinal fluid was cytocentrifuged (GP centrifuge; Beckman, Fullerton, CA) onto a glass slide coated with poly-L-lysine (P4832; Sigma-Aldrich, St. Louis, MO) at the bottom of a 24-well multiwell plate (BD Falcon, Bedford, MA) at 1500 rpm for 10 minutes. Supernatant was removed. Subsequently, the cells were incubated at 37°C in RPMI 1640 medium containing 10% FBS. After incubation for 3 hours, the cells were washed three times with PBS and fixed in acetone/methanol (2:3) for 10 minutes at −20°C. After blocking nonspecific protein in 0.1% BSA in PBS for 30 minutes at room temperature, primary antibody CD68 (ab845; Abcam, Cambridge, UK) was applied for 3 hours at room temperature, and secondary antibody (Alexa Fluor 647; Invitrogen, Carlsbad, CA) was applied for 30 minutes at room temperature. The negative control was without secondary antibody. Immunofluorescence-labeled and differential interference images were obtained (LSM510 META; Carl Zeiss Meditec, Dublin, CA). The emission fingerprint of fluorescence was also recorded using the lambda META scanning mode, in which fluorescence in a 10-nm width is recorded by a polychromatic 8-channel detector that allows fast acquisition of lambda stacks. Fluorescence was excited by an Ar^+ laser for 458, 488, and 514 nm; an HeNe laser for 532 nm excitation; and an HeNe laser for 633-nm excitation through an appropriate dichroic mirror. To compare the emission fingerprint, the detector gain and excitation light intensity were set constant for a set of experiments. The fluorescence intensity profile was exported as text and used to analyze the peak, by using the local maximum method in the peak-finding module of the software (Origin 8; OriginLab Corp., Northampton, MA).

RESULTS

Identification of Cells

The ages of the patients with RRD were 11, 17, and 24 years (Table 1). Preoperative examination revealed yellow precipitates and corresponding granular autofluorescence on the outer surface of the retina in all three eyes with long-standing RRD. All eyes with retinal detachment had subretinal strands that showed hyperautofluorescence (Fig. 1). The eye with Coats' disease in a 15-year-old boy showed diffuse hyperautofluorescence in the area of bullous retinal detachment. Part of hyperautofluorescence appeared as spotted hyperautofluorescent lesions between the retinal folds (Fig. 2).

The cells from the subretinal space were classified into three types. The first type was relatively large, round cells that had

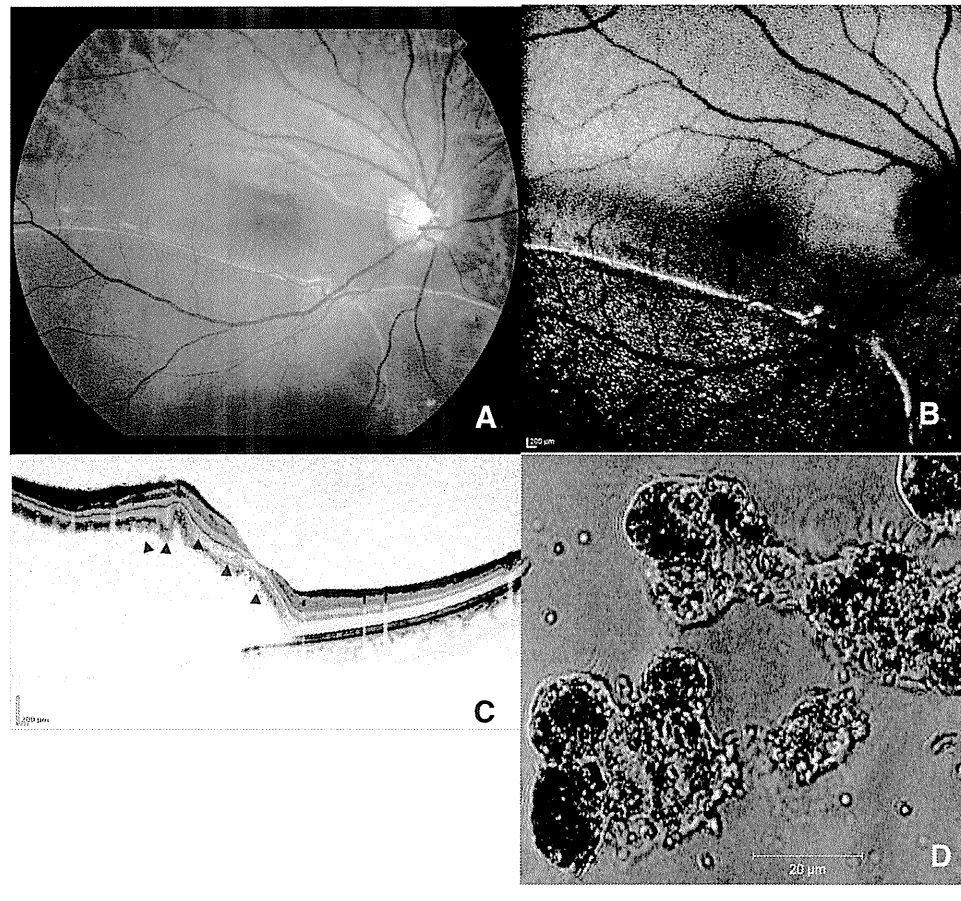

FIGURE 1. A 24-year-old man. The right eye showed long-standing retinal detachment with a subretinal strand (**A**). FAF demonstrated granular hyperautofluorescence within retinal detachment (**B**). The subretinal strand also showed strong granular hyperautofluorescence. OCT revealed low signal intensity dots on the outer retinal surface or in the retina (*arrowheads*) (**C**). Differential interference image of the pigmented cells in subretinal fluid (**D**).

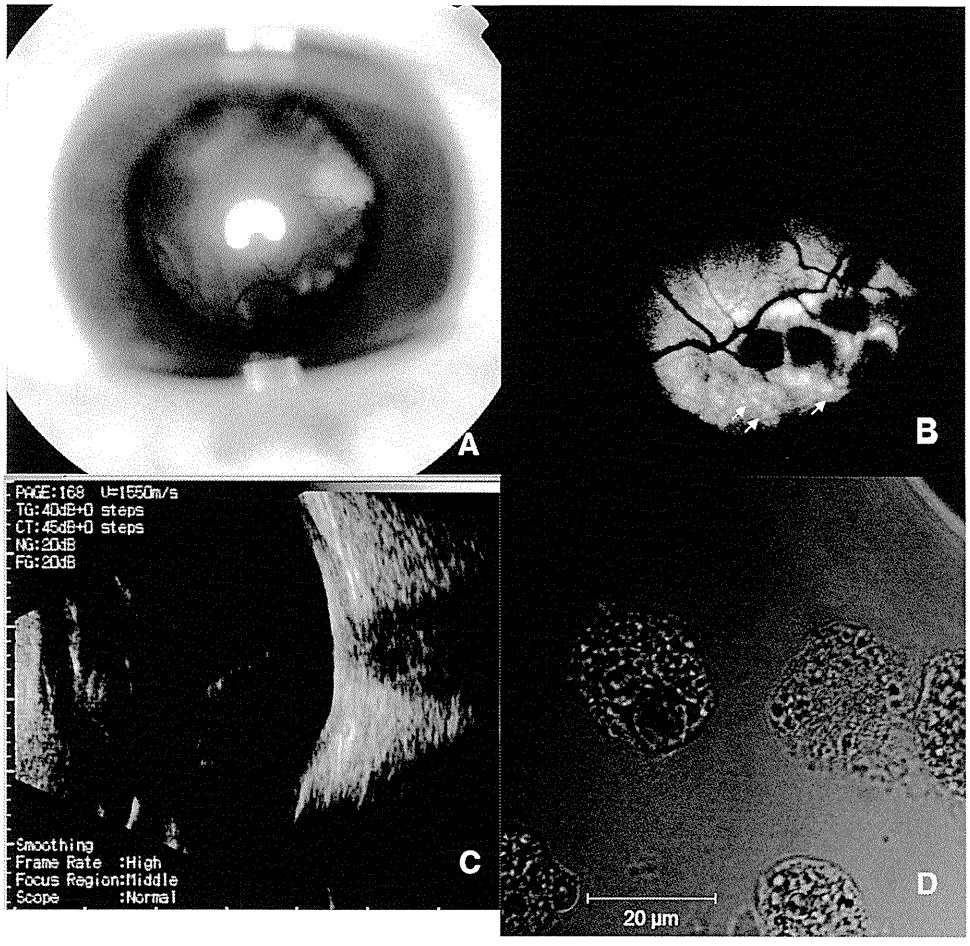

FIGURE 2. A 15-year-old boy. The left eye showed bullous retinal detachment with a yellow subretinal deposit (**A**). Fundus autofluorescence demonstrated diffuse hyperautofluorescence (**B**). Ultrasonography showed bullous retinal detachment (**C**). Large cells in the subretinal fluid with few pigment granules were observed by differential interference microscopy (**D**). Some spotted hyperautofluorescent lesions appeared between the retinal fold (*arrow*).

well-defined cytoplasm and nuclei covered with numerous pigments. Heavily pigmented cells were negative for CD68 staining. Autofluorescent inclusions appeared in the cytoplasm (Fig. 3). This type of cell frequently appeared in the specimens of the RRD cases. The second type was large (20–50 μm in diameter), rounded or polygonal cells with few or no pigments. Differential interference contrast microscopy showed various sizes of vacuoles in the cytoplasm. Most of the subretinal cells in the eye with Coats' disease were positive for CD68 staining (patient 4). The contour of vacuoles was clearly observed when the cells were stained immunocytochemically. Autofluorescent inclusions appeared in the cytoplasm and in some vacuoles (Fig. 4). This type of cell appeared more frequently in the specimens from the subretinal fluid of Coats' disease. The third type of cell is the spindle-shaped or oval cells that had few or no pigments in the cytoplasm. These cells were negative for CD68 staining and did not show autofluorescence. The density of each type of the cells was summarized in Figure 5.

Fluorescence Spectroscopy

Fluorescence spectroscopy was applied to the first two types of cells. The intensity of autofluorescence of inclusions in the cells with CD68-positive or -negative cells stained with anti-CD68 antibody probed by AlexaFluor-647-labeled secondary antibody was examined with various excitation lights (458, 488, 514, 543, and 633 nm). The cells were characterized by the presence of far-red to infrared fluorescence excited by a 633-nm laser (Figs. 6I, 6J). Unexpectedly, when excited by a 458- or 488-nm laser light, emission spectra of autofluorescence showed little difference, either in CD68-positive or -negative cells (Figs. 6A–D). The emission peak at 580 nm was comparable in either type of cell. Red fluorescence obtained by excitation with longer wavelengths (514 and 543 nm) was higher in CD68-positive cells (Figs. 6E–H), but the CD68-negative cells still showed significant autofluorescence. We could not find any remarkable difference in the spectra between the cells from the eyes with RRD and that from the eye with Coats' disease. To obtain quantitative information, peak analysis was performed for each emission curve on a total of 50 autofluorescent inclusions in four to six typical cells from each of the four specimens (Table 2). Consistent with Figure 6, this analysis also indicates that almost all CD68-negative cells contain apparent autofluorescent vesicles, demonstrating that autofluorescence does not associate with CD68 expression. In the 458- and 488-nm emission spectra, the cells classified as the former two types showed the narrow peak at the same wavelength.

DISCUSSION

Characteristics of autofluorescence were examined in the cells collected from subretinal fluid in eyes with retinal detachment, which showed autofluorescence in the area of retinal detachment. The cells were classified morphologically and immunocytologically, with CD68 used as the marker for macrophages. We found that autofluorescent inclusions appeared in the CD68-positive cells and -negative cells. No clear difference in autofluorescence spectra was observed in the two types of cells.

Although the main origin of FAF is lipofuscin in the retinal pigment epithelium, the subretinal deposits also show autofluorescence in eyes with retinal detachment caused by RRD,[22] central serous chorioretinopathy,[8,10,11,23] Best's disease,[4,24] age-related macular degeneration,[25] or choroidal hemangi-